

DESIGNING, TESTING AND MODELLING TWO INNOVATIVE NON-CONVENTIONAL BUCKLING RESTRAINED BRACES FOR SEISMIC RESISTANT BUILDINGS

Daniel Piedrafita Francos

Dipòsit legal: Gi. 1800-2014
<http://hdl.handle.net/10803/284738>



<http://creativecommons.org/licenses/by/4.0/deed.ca>

Aquesta obra està subjecta a una llicència Creative Commons Reconeixement

Esta obra está bajo una licencia Creative Commons Reconocimiento

This work is licensed under a Creative Commons Attribution licence



UNIVERSITAT DE GIRONA

DESIGNING, TESTING AND
MODELLING TWO INNOVATIVE
NON-CONVENTIONAL BUCKLING
RESTRAINED BRACES FOR SEISMIC
RESISTANT BUILDINGS

DOCTORAL THESIS

2014

Daniel Piedrafita Francos



UNIVERSITAT DE GIRONA

DESIGNING, TESTING AND MODELLING TWO
INNOVATIVE NON-CONVENTIONAL BUCKLING
RESTRAINED BRACES FOR SEISMIC RESISTANT
BUILDINGS

DOCTORAL THESIS

2014

Daniel Piedrafita Francos

Supervisor: Xavier Cahís i Carola

Doctorat en Tecnologia

THESIS SUBMITTED FOR THE DEGREE OF DOCTOR OF PHILOSOPHY BY THE
UNIVERSITAT DE GIRONA

A la meua família i amics, per la seva estima

”Ningú ens va dir que hi anéssim, ningú ens va dir que ho intentéssim, ningú ens va dir que seria fàcil. Algú va dir que som els nostres somnis, que si no somiem estem morts. Els nostres passos segueixen l’instint que ens porta al desconegut, no mirem els obstacles que hem superat sinó aquells que superarem ...”

Kilian Jornet

Acknowledgements //

Agraïments // Agradecimientos

I would like to express my gratitude to the AMADE research group of the University of Girona and to Bellapart SAU for believing in our project and for giving us the opportunity to develop it.

També vull agrair al meu director Xavier Cahís la seva dedicació i les bones idees que ha tingut, té i tindrà, per ensenyar-me i deixar-me agafar responsabilitats en els assaigs, i sobretot li vull agrair l'esforç que ha fet quan les coses no han anat bé, per no triar mai el camí fàcil de deixar-les passar, per sempre voler que la feina estigui ben feta. Encara que de vegades no t'ho he posat fàcil, gràcies Xavier.

Agrair també a en Pere Maimí la seva ajuda i dedicació, per tot el que he après d'ell i perquè estic orgullós del resultat.

Moltes gràcies als companys d'AMADE amb els que he compartit alegries, penes i desitjos de futur al voltant d'una tassa de cafè. Per tot el que he après de vosaltres i perquè vam començar sent companys i per mi ara sou amics.

A la gent dels tallers de la politècnica: en Jordi, en Sergi i en Pere. Per la vostra paciència amb “el de la bata blanca”, per tot el que m'heu ensenyat i per les xerrades de passadís.

Agradezco a la gente del CeReDeTeC de la Universidad Tecnológica Nacional Facultad Mendoza el permitirme hacer la estancia con ellos. Especialmente agradecerle a Gustavo la oportunidad de ir y la de trabajar con él. A la gente del laboratorio, mención especial a Claudio y a Jonny por sacarme a pasear y a Marcelo y a Sergio por los mates con las clases de “argentinidad”. A Víctor y a Pancho por los viajes a San Juan (jeje). También a toda la gente de Mendoza que me hizo sentir como en casa: A Tuiti, a El Gordo y a Nao por dejarme descubrir los Andes con ellos. A todo el grupo de los trekkings y trotes: Selva, Noe, Vivi, Coqui, Silvana, Norma, Beta y demás. A Beta, a Pao y a Mechas por los vinos, las risas y los buenos ratos que compartimos.

Als de La Colla perquè cadascun de vosaltres fa de la meva vida un lloc un mica més feliç, per tot el que hem compartit i compartirem!

Als Apòstols de Bacus per les bones estones de muntanya i les que encara ens queden!

Als meus pares, a l'Olga i a en Carles, perquè sempre heu estat allà, i encara que de vegades em costi expressar-ho: us estimo molt.

També agrair a tots aquells que en algun moment els nostres camins s'han creuat i m'heu fet partícip de la vostra felicitat.

Perquè la tesi no és un punt i final, si no un punt i seguit, que continui la diversió!

The present work has been funded by Bellapart SAU and the AMADE research group of the University of Girona under research grant BRGR 11-09.

This Ph.D. thesis has been prepared as a compendium of papers, according to the regulations of the University of Girona (*Normativa d'ordenació dels ensenyaments universitaris de doctorat de la Universitat de Girona, aprovada pel Consell de Govern en al sessió 3/12, de 26 d'abril de 2012, i modificada pel Consell de Govern en la sessió 5/2013, de 25 de setembre de 2013*). This thesis includes three original papers: One paper that has already been published in a peer-reviewed journal, and another two have already been submitted.

The complete references of the papers comprising this thesis, the impact factors, quartile, and category of the journals are:

Daniel Piedrafita; Xavier Cahis; Enric Simon; Jordi Comas. *A new modular buckling restrained brace for seismic resistant buildings*. Engineering Structures 2013; 56; 1967-1975

ISSN: 0141-0296

doi: 10.1016/j.engstruct.2013.08.013

(Impact index 1,713. Journal 18 of 122, 1st quartile, Category: Engineering, Civil)

Daniel Piedrafita; Xavier Cahis; Enric Simon; Jordi Comas. *A new slotted buckling restrained brace*. Submitted to Engineering Structures.

(Impact index 1,713. Journal 18 of 122, 1st quartile, Category: Engineering, Civil)

Daniel Piedrafita; Pere Maimí, Xavier Cahis. *A constitutive model for simulating all-steel buckling restrained braces* Submitted to Engineering Structures.

(Impact index 1,713. Journal 18 of 122, 1st quartile, Category: Engineering, Civil)

The three papers have been published (or submitted to) journals with impact factors within the first quartile, according to the 2013 Journal Citation Reports.

To whom it might concern,

Dr. Xavier Cahís i Carola, Professor at the University of Girona of the Department of *Enginyeria Mecànica i de la Construcció Industrial*

CERTIFIES that the study entitled *Designing, testing and modelling two innovative non-conventional buckling restrained braces for seismic resistant buildings* has been carried out under his supervision by *Daniel Piedrafita Francos* to apply for the doctoral degree with International Mention.

Girona, July 2014

Dr. Xavier Cahís i Carola
Universitat de Girona, Spain

List of Figures

1.1	Scheme of conventional structure [45]	2
1.2	Elastomeric bearings [22]	3
1.3	Sliding friction pendulum [22]	3
1.4	Scheme of structure with passive system (PED) [45]	4
1.5	Scheme of structure with active system [45]	4
1.6	Scheme of structure with hybrid system [45]	5
1.7	Scheme of structure with semi-active system [45]	5
1.8	Schematic representation of rate-dependent and rate-independent passive systems [47]	6
1.9	Added Damping and Stiffness (ADAS) dissipator [9]	7
1.10	Scheme of the installation of Buckling Restrained Braces and the concept of inter-story drift	8
1.11	Hysteretical response of non buckling restrained frame and buckling restrained frame	9
1.12	Scheme of the transversal section of a conventional Buckling Restrained Brace	9
2.1	Schematic description of the conventional BRB	16
2.2	a) Modular Buckling Restrained Brace (MBRB) core geometry b) Seriated Module (SM) detail	19
2.3	Scheme of a Modular Bucking Restrained Brace (MBRB)	20
2.4	Working scheme of a Shear Basic Dissipation Unit (SBDU), internal forces distribution and shear deformation	20
2.5	γ_m definition, Cahís [18]	22
2.6	Effects of the geometrical imperfections on the end connections	23
2.7	Idealized variable cross-section bar [4]	24
2.8	Scheme of test set-up	26

2.9	Push protocols: a)AISC341-05[2] protocol b)EN15129[5] protocol c)Cyclic deformation with increasing amplitude	26
2.10	Core transducers localization	26
2.11	Force versus total deformation of each specimen core	27
2.12	Experimental response of each Seriated Module (SM) a) Specimen 1 b) Specimen 2 c) Specimen 3	28
2.13	Linear correlation between the ultimate force ($F_{SBDU,u}$) and Shear Basic Dissipation Unit ductility (μ_{SBDU})	29
2.14	Cumulated Shear Basic Dissipation Unit Ductility ($\mu_{SBDU,cum}$) vs. Shear Basic Dissipation Unit Ductility (μ_{SBDU})	30
2.15	Stress distribution at maximum displacement of the FEM model, specimen 1	32
2.16	Experimental vs. numerical response	32
3.1	Scheme of conventional buckling restrained brace parts	37
3.2	a) and b)sections of conventional BRB, c) all-steel BRB and slotted buckling restrained brace d)	39
3.3	Brace assembly	39
3.4	Slotted buckling restrained brace core, lateral bands in red, stabi- lizing bridges in blue.	39
3.5	Key dimensions of the core	40
3.6	Test set-up, restraining unit parts and external displacement trans- ducer positions	41
3.7	Internal transducer position	42
3.8	Experimental specimens: a) Type I b) Type II	43
3.9	Experimental results and applied push protocols	44
3.10	Failure mechanism of the specimens. Ex: External zone, In: In- ternal zone	44
3.11	Cumulated ductility($\mu_{c,cum}$) vs ductility(μ_c)	45
3.12	Numerical model parts and mesh	47
3.13	Contour conditions of the core	47
3.14	Comparison between the hysteretic behaviour of the numerical model and specimen I.3 during the first cycles	48
3.15	Numerical vs experimental behaviour at the yielding point of spec- imen I.3	48

3.16	Core stress distribution of specimen I.3 at peak tension force on the third test cycle	49
3.17	Evolution of the axial strains from the FEM analysis of specimen I.3	50
3.18	Deformation under tension force of numerical model of specimens I.3 and II.3 after several cycles	50
3.19	Out-plane and in-plane (δ_{IP}) displacement of the numerical model of specimen I.3 after several cycles	51
3.20	In-plane displacement vs the core deformation for FEM models of the specimens I.1 and II.1	51
4.1	Comparison between the behaviour of the restraining brace without a) and with b) the encasing member	57
4.2	a)ABAQUS [7] isotropic hardening model and b)ABAQUS [7] combined hardening model applied to MBRB [41]	59
4.3	Evolution of the yielding surface	60
4.4	Response of the modelled material vs. an experimental result from the tensile test. The evolution of damage variable (D) in the central element of the necking is in grey	64
4.5	(a) Modular Buckling Restrained Brace core geometry (b) Seriated Module (SM) detail [41]	65
4.6	(a) AISC341-05 [2] protocol (b) EN15129 [5] (c) cyclic deformation with increasing amplitude [41]	66
4.7	Mesh and boundary conditions of the numerical model	67
4.8	Comparison between experimental and numerical behaviour of the three specimens	67
4.9	a) Photo after failure of tested specimen b) Amount of plastic flow (r) and c) Damage variable (D) distribution at maximum displacement on traction of numerical model of specimen 3	68
4.10	Damage variable (D) evolution compared with core deformation (u)	69

List of Tables

2.1	Average thickness of Shear Basic Dissipation Units (SBDUs) (t_w)	27
2.2	Summary of experimental results	29
2.3	Comparison of normalized hysteretic energy (E_t^*), normalized cumulative plastic deformation (μ_{cum}^*) and maximum tension and compression forces between a MBRB and a conventional BRB (Newell et al. [36])	30
2.4	Material properties of the numerical model	31
2.5	Comparison between experimental, analytical and numerical results, specimen 1	32
3.1	Summary of the experimental results of the specimens	46
3.2	Comparison between an SBRB and conventional BRBs [36]. Normalized hysteretic energy (E_t^*), cumulative deformation ($\mu_{b,cum}$) and coefficient β	46
3.3	Material data used on numerical model	47
3.4	Comparison between the analytical, experimental and numerical values at the yielding point	49
4.1	Constant values of the material	64
4.2	Constant values of damage model [42]	64
B.1	Material parameters	86
B.2	ABAQUS input material parameters and internal variables	87
B.3	Internal variable meanings	88

Contents

Abstract	xi
1 Introduction and objectives	1
1.1 Introduction	2
1.2 Structural response control	2
1.2.1 Passive energy dissipators	5
1.2.2 Key issues in conventional Buckling Restrained Braces	7
1.3 Non-conventional Buckling Restrained Braces	9
1.4 Modelling buckling restrained braces	10
1.5 Objectives	11
2 A new modular buckling restrained brace for seismic resistant buildings	13
2.1 Notations	15
2.2 Introduction: Buckling Restrained Braces	16
2.3 The Modular Buckling Restrained Brace. The concept and design parameters	18
2.4 Design parameters of the Shear Basic Dissipation Unit	21
2.5 Restraining tube design	22
2.6 Experimental behavior	25
2.6.1 Test set-up and push protocols	25
2.6.2 Tested specimens	27
2.6.3 Experimental results	27
2.7 Numerical prediction	31
2.8 Summary and conclusions	33
2.9 Acknowledgements	34

3	A new slotted buckling restrained brace	35
3.1	Introduction	37
3.2	Slotted buckling restrained brace	38
3.3	Test set-up and push protocols	41
3.4	Experimental results	43
3.5	Numerical analysis	46
3.6	Summary and conclusions	51
3.7	Acknowledgements	53
4	A constitutive model for simulating all-steel buckling restrained braces	55
4.1	Introduction	57
4.2	Constitutive model	59
4.2.1	Plasticity	59
4.2.2	Damage	60
4.3	Implementation	61
4.3.1	Algorithm	61
4.3.2	Tangent operator	62
4.4	Model adjustment	62
4.5	Modelling of an all-steel BRB	64
4.6	Summary and conclusions	69
4.7	Acknowledgements	70
5	Discussion and conclusions	71
	Appendixes	75
A	Published paper: A new modular buckling restrained brace for seismic resistant buildings	75
B	User material implementation for all-steel BRBs	85
B.1	Preface	86
B.1.1	ABAQUS input file	86
B.1.2	State variables	88
B.2	Code	88
	Bibliography	96

Abstract

Advanced seismic design based on structural response control allows the damage buildings experience under seismic actions to be reduced. Several solutions have been developed and implemented around the world. Buckling Restrained Braces (BRB) are one of them. BRBs are inertial response devices whose metallic core yields in order to dissipate earthquake energy. They are installed in the structure like conventional restraining braces, but as their yielding core is such a slender element a restraining unit is required to avoid the brace buckling under compression forces. In conventional BRBs this element is composed of a steel hollow profile filled with mortar to achieve dimensional compatibility between the core and the encasing member. The use of mortar requires the use of a debonding material between the restraining unit and the core to minimize the friction force between them and allow the free lateral expansion of the core when it is compressed. BRBs filled with mortar have been proven to be effective dissipation devices but they have several shortcomings: they are heavy which complicated mounting tasks and increases the seismic inertial forces, the core can not be inspected or substituted if necessary, after severe earthquakes, and they are expensive to manufacture. All-steel BRBs are BRBs where the core is restrained by a restraining unit composed of steel profiles, welded or bolted, in an attempt to solve some of the above-mentioned shortcomings of conventional BRBs.

In this work, two all-steel BRBs are developed. These non-conventional BRBs are composed of a stabilized metallic yielding core and a slotted restraining unit manufactured with several steel bars which are welded to form a hollow element providing a guiding element to the core. One of them is the Modular Restrained Brace (MBRB). The main difference between the MBRB and conventional BRBs is found in the core as is designed to transmit the axial force by shear deformations in modularly connected shear dissipation units. The second new BRB developed is the Slotted Buckling Restrained Brace (SBRB). Its yielding core yields under

axial strains, as conventional BRBs do, but the yielding take place in the lateral bands situated in the outer zone of the core. Its yielding core consists of a perforated plate with two lateral bands coupled by stabilizing bridges. The buckling of the lateral bands is prevented by the restraining unit and the stabilizing bridges. Both new BRB designs allow the core to be inspected and replaced if damaged. For both non-conventional BRBs, analytical expressions to size it have been developed, testing based on two codes have been carried out and simplified numerical models to reproduce approximately their behaviour have been made.

Currently, the only way to characterize BRBs, as outlined by the codes, are through full-scale tests. These tests involve a lot of work and they are expensive. Thanks to today's computational capacity the models using the Finite Element Method (FEM) are able to simulate the entire BRB and the interactions between its elements. However, as the BRBs yielding cores are submitted to low cycle phenomena with large plastic deformations, the available material models in commercial FEM are not able to properly reproduce the hysteretic behaviour of the BRBs. In this work a constitutive model for simulating all-steel buckling restrained braces is presented. The plastic region of this model is formulated using a combination of isotropic and kinematic hardening, the portion of each being related to the amount of plastic flow. The damage is introduced as a post-process variable using an existing model based on continuum damage mechanisms.

Resum

El disseny avançat d'estructures basat en la resposta estructural permet reduir el dany que experimenten els edificis sota les accions sísmiques. Diverses solucions s'han desenvolupat i implementat arreu del món. Els Braços de Vinclament Restringit (BVR) són una d'elles. Els BVR són dispositius de resposta inercial que són capaços de dissipar l'energia provinent del sisme a través de la plastificació del seu nucli metàl·lic. S'instal·len a l'estructura com els braços de travat convencionals, però com que el seu nucli és un element esvelt el seu vinclament sota forces de compressió ha de ser evitat mitjançant un element de travat. En els BVR convencionals aquest element està format per un perfil tubular d'acer ple de morter que permet aconseguir la compatibilitat dimensional entre el nucli dissipador i l'element de travat. L'ús del morter obliga també a l'ús d'un material separador entre l'element de travat i el nucli per evitar la interacció entre ells i permetre l'expansió lateral del cor quan es troba sota compressió. Els BVR plens de morter han demostrat ser uns dispositius dissipadors d'energia efectius, però presenten diversos inconvenients: són pesats amb un muntatge complicat i incrementen les forces sísmiques inercials, el nucli no pot ser inspeccionat, ni substituït si fos necessari, després de sismes severos, a més són cars de fabricar. Els BVR metàl·lics són BVR on el nucli està restringit per un element de travat format per perfils metàl·lics, ja siguin soldats o cargolats, en un intent de solucionar alguns dels inconvenients abans mencionats dels BVR convencionals.

En aquest treball s'han desenvolupat dos BVR totalment metàl·lics. Aquests BVR no convencionals estan formats per un nucli metàl·lic estabilitzat per un element de travat ranurat fabricat soldant perfils metàl·lics formant una secció tancada. Un d'ells és el Braç de Vinclament Restringit Modular (BVRM). La principal diferència entre aquest i els BVR convencionals és que està dissenyat per transmetre les forces axials mitjançant deformacions tallants a través d'unitats de dissipació a tallant connectades de manera modular. El segon nou BVR

desenvolupat és el Braç de Vinclament Restringit Ranurat (BVRR). El seu nucli plastifica sota deformacions axials, com el dels BVR convencionals, però la plastificació té lloc en les bandes laterals situades en la part exterior del nucli. Aquest nucli dissipador consisteix en una platina perforada amb les dues bandes laterals unides pels ponts estabilizadors. El vinclament d'aquestes bandes laterals està impedit per l'element de travat ranurat i per la resta del nucli. Els dissenys dels dos nous BVR permeten inspeccionar i substituir els nuclis en cas d que estiguin danyats. Pels dos BVR no convencionals, s'han desenvolupat expressions analítiques pel seu dimensionat, s'han portat a terme assaigs d'acord amb dues normes i s'han fet models numèrics simplificats que reproduïen de manera aproximada el seu comportament.

Avui en dia, l'únic camí per a caracteritzar els BVR, tal i com marquen les normatives, són els assaigs a escala real. Aquests assaigs impliquen molta feina i són cars. Gràcies a la capacitat computacional actual els models usant el Mètode dels Elements Finitos (MEF) són capaços de simular els BVR complets, així com les interaccions entre els elements que els formen. Però com que els nuclis dels BVR estan sotmesos a un fenomen de fatiga per baixos cicles amb grans deformacions plàstiques, els models de material disponibles en els MEF comercials no són capaços de reproduir de manera adequada el comportament histerètic del BVR. En aquest treball es presenta un model constitutiu per a la simulació de BVR metàl·lics. La regió plàstica d'aquest model s'ha formulat utilitzant una combinació d'enduriment isotròpic i cinemàtic, la porció de cadascun és funció de la quantitat de deformació plàstica. El dany és introduït com una variable de post-procés fent servir un model existent basat en els mecanismes de dany continu.

Resumen

El diseño avanzado de estructuras basado en la respuesta estructural permite reducir el daño que experimentan los edificios sometidos a las acciones sísmicas. Diversas soluciones se han desarrollado e implementado por todo el mundo. Las Barras de Pandeo Restringido (BPR) son una de ellas. Las BPR son dispositivos de respuesta inercial capaces de disipar la energía que proviene del seísmo mediante la plastificación de su núcleo metálico. Se instalan en la estructura como los brazos de trabado convencionales pero como su núcleo es un elemento esbelto, su pandeo bajo fuerzas de compresión tiene que ser evitado mediante el uso de un elemento de trabado. En las BPR convencionales este elemento está formado por un perfil tubular de acero relleno de mortero para asegurar la compatibilidad dimensional entre el núcleo y el elemento de trabado. El uso de mortero obliga también al uso de un material separador entre el elemento de trabado y el núcleo para evitar la interacción entre ellos y permitir la expansión lateral del núcleo bajo compresión. Las BPR han demostrado ser unos dispositivos disipadores de energía efectivos, pero presentan diversos inconvenientes: son pesados con un montaje complicado y incrementan las fuerzas sísmicas inerciales, el núcleo no puede ser inspeccionado, ni substituido si fuera necesario, después de sismos severos, además son caros de fabricar. Las BPR metálicas son BPR donde el núcleo está restringido por un elemento de trabado formado por perfiles metálicos, ya sean soldados o atornillados, en un intento de solucionar algunos de los inconvenientes anteriormente mencionados de las BPR convencionales.

En este trabajo se han desarrollado dos BPR totalmente metálicas. Estas BPR no convencionales están formadas por un núcleo metálico estabilizado mediante un elemento de trabado ranurado fabricado soldando perfiles metálicos formando una sección cerrada. Una de ellas es la Barra de Pandeo Restringido Modular (BPRM). La principal diferencia entre esta y las BPR convencionales es que esta diseñada para transmitir las fuerzas axiales mediante deformaciones cortantes

a través de unidades de disipación a cortante conectadas de manera modular. La segunda nueva BPR diseñada es la Barra de Pandeo Restringido Ranurada (BPRR). Su núcleo plastifica bajo deformaciones axiales, como en las BPR convencionales, pero la plastificación ocurre en las bandas laterales situadas en la parte exterior del núcleo. Este núcleo disipador consiste en una pletina perforada con las dos bandas laterales unidas por los puentes estabilizadores. El pandeo de estas bandas laterales está impedido por el elemento de trabado y el resto del núcleo. Para las dos BPR no convencionales se han desarrollado expresiones analíticas para su dimensionado, se han llevado a cabo ensayos de acuerdo con dos normas y se han realizado modelos numéricos simplificados que reproducen de manera aproximada su comportamiento.

Hoy en día, el único camino para caracterizar las BPR, tal y como marcan las normativas, son los ensayos a escala real. Estos ensayos implican mucho trabajo y son caros. Gracias a la capacidad computacional actual los modelos usando el Método de los Elementos Finitos (MEF) son capaces de simular las BPR completas, así como las interacciones entre los elementos que las forman. Pero como los núcleos de las BPR están sometidos a un fenómeno de fatiga por bajos ciclos con grandes deformaciones plásticas, los modelos de material disponibles en los MEF comerciales no son capaces de reproducir de manera adecuada el comportamiento histerético de las BPR. En este trabajo se presenta un modelo constitutivo para la simulación de BPR metálicas. La región plástica de este modelo se ha formulado utilizando una combinación de endurecimiento isotrópico y cinemático, la porción de cada uno de ellos es función de la cantidad de deformación plástica. El daño es introducido como una variable de post-proceso utilizando un modelo existente basado en los mecanismos de daño continuos.

Chapter 1

Introduction and objectives

1.1 Introduction

In the present chapter, there is firstly a general introduction about structural response control followed by a summary of the thesis contents and finally the main objectives of this work are introduced.

This thesis has been prepared as a compendium of papers. Chapter 2 contains a transcription of the published paper "A new modular buckling restrained brace for seismic resistant buildings". This paper, in journal format, is shown in Appendix A. Chapter 3 is a transcription of a submitted paper "A new slotted buckling restrained brace". Finally, Chapter 4 consists of a transcription of the submitted paper "A constitutive model for simulating all-steel buckling restrained braces".

The last chapter is composed of a discussion and the conclusions of the preceding chapters along with some suggested future work.

1.2 Structural response control

Earthquakes generate and transfer a large amount of energy input into building structures. With the traditional design method, a building withstands this by means of the strength of its columns and beams Fig. 1.1. This design takes advantage of member ductility and structural redundancy to develop plastic hinges and to dissipate the energy input [23]. However, in severe earthquakes, structural elements suffer damage and although this does not cause collapse, this damage would be difficult to repair.

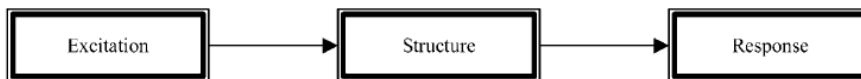


Figure 1.1: Scheme of conventional structure [45]

Nowadays, design based on structural response control offers several ways to improve the response of structures under seismic actions. Soong and Spencer [45] classified these options into three families, namely base isolation, passive energy dissipation and active control. Other authors [17] include base isolation in the passive protective systems and divide the family of active control systems into hybrid protective systems and active protective systems.

When compared with the other solutions, base isolation is considered the more mature technology. In addition, as the main objective of the seismic isolation design is to uncouple the structure from the ground and avoid the effects of earthquake ground motion, this is why some authors separate it from passive systems. Base isolators are particularly effective for retrofitting low and stiff buildings, such as historical masonry buildings [17]. According to Soong [44] base isolation is made up of three main technologies: Elastomeric bearings, lead rubber bearings (Fig. 1.2) and a sliding friction pendulum (Fig. 1.3).

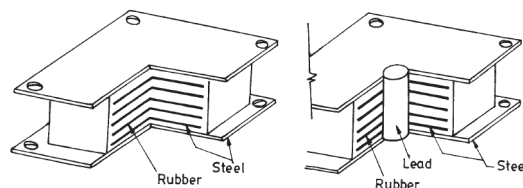


Figure 1.2: Elastomeric bearings [22]

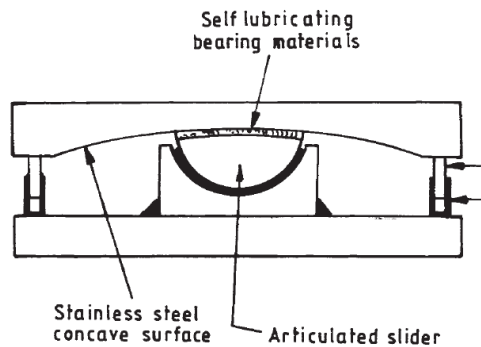


Figure 1.3: Sliding friction pendulum [22]

Passive systems (Fig. 1.4) enhance damping, stiffness and the strength of the structure. They are characterized by their inertial response and for this reason they do not need an external energy supply. They increase the energy dissipation capacity of the structural system. They mainly operate on principles such as the yielding of the metals, phase transformation in metals, deformations of viscoelastic solids, fluid orificing or frictional sliding. In the next section the various solutions that exist will be described.

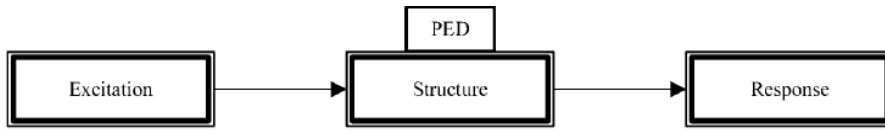


Figure 1.4: Scheme of structure with passive system (PED) [45]

Active control systems (Fig. 1.5) are force delivery devices integrated with real-time sensors, processing devices and controllers within the structure. They provide an external force which is based on the external excitation (earthquake or wind) and/or the structural response. However, despite their cost effectiveness ratio and reliability, their wide-spread acceptance is limited because of their dependency on energy supply.

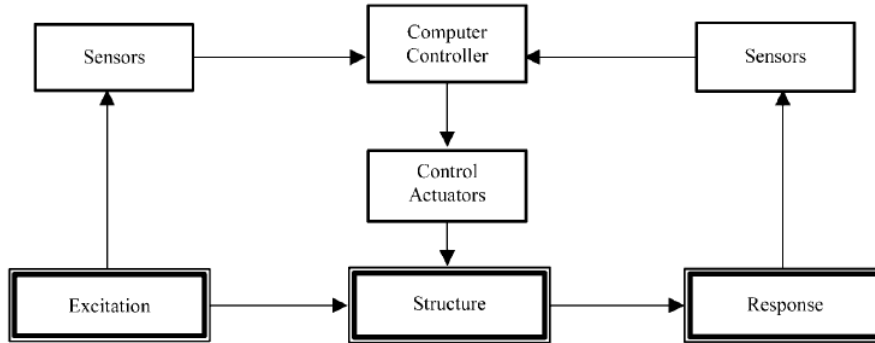


Figure 1.5: Scheme of structure with active system [45]

Hybrid systems (Fig. 1.6) are defined by Soong and Spencer [45] as a combination of a passive and active control system. Since a portion of the control objective is accomplished by the passive system, this results in less active control effort, implying less power resource is required.

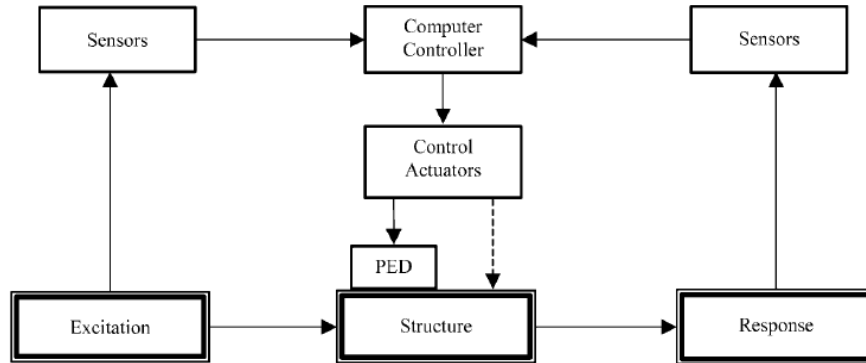


Figure 1.6: Scheme of structure with hybrid system [45]

Semi-active systems (Fig. 1.7) are an attractive alternative to active and hybrid systems because of their mechanical simplicity, low power requirements and large force capacity. Spencer and Nagarajaiah [46] define a semi-active control device as one which cannot inject mechanical energy into the controlled structural system, but the device's properties are controlled in real-time to improve the responses of the system.

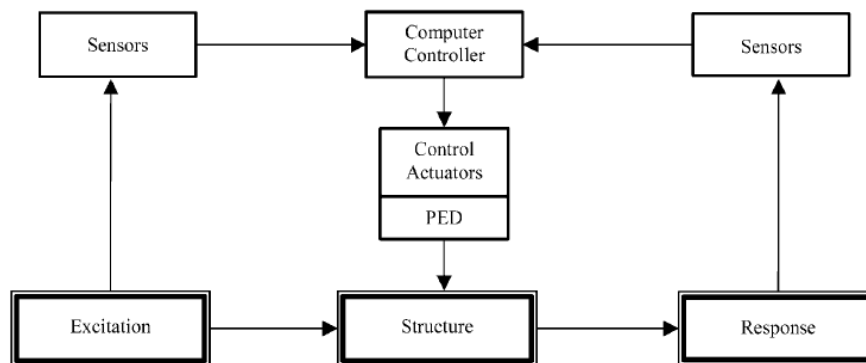


Figure 1.7: Scheme of structure with semi-active system [45]

1.2.1 Passive energy dissipators

Several solutions for passive energy dissipators have been developed. Symans et al. [47] classified energy dissipators into three categories: 1) rate-dependent devices 2) rate-independent devices 3) others. In the rate-dependent devices the force output depends on the rate of displacement changing. Examples of these are the viscoelastic solid or fluid dampers. Viscous fluid dampers are based on using a cylinder with a fluid forced to flow through orifices. Viscoelastic solid dampers

use elastomeric pads working under shear strain. With the rate-independent devices the force response is only dependent on the magnitude of the displacement. Typically these devices are metallic or friction dampers [44]. Fig. 1.8 shows a schematic description of these systems and their hysteretical response. Metallic dampers use the yielding of the metal, both under flexure, axial or shear stresses to dissipate earthquake energy. Friction dampers, dissipate energy through the friction between two solid bodies. Other options include tuned mass and liquid dampers and phase transformation dampers [43].

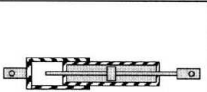
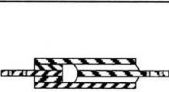
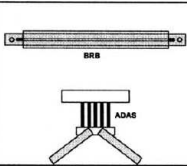
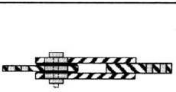
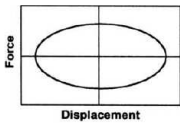
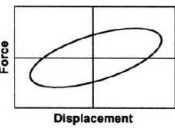
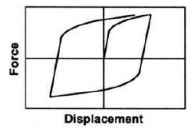
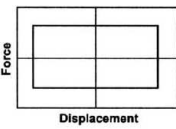
	Viscous Fluid Damper	Viscoelastic Solid Damper	Metallic Damper	Friction Damper
Basic Construction				
Idealized Hysteretic Behavior				

Figure 1.8: Schematic representation of rate-dependent and rate-independent passive systems [47]

The metallic dampers are widely used because they offer a good hysteretical response and their properties are easier to ensure, even a long time after installation, than other options such as the friction dampers. The use of the yielding of metals to design energy dissipators is a wide-spread solution. Several designs have been developed and tested, although, according Symans et al. [47], Added Damping and Stiffness (ADAS) and Buckling Restrained Braces (BRB) are the two most commonly used types.

ADAS dampers [9, 51] is a system composed of several X-shaped steel plates installed in parallel between the top and bottom connections (see Fig. 1.9). The geometry of the plates (in double curvature) allow uniform strains along this height when submitted to bending moments induced by the shear forces caused by the relative motion between the two consecutive floors (see inter-story drift definition in Section 1.2.2). So these devices are able to dissipate a large amount of energy.

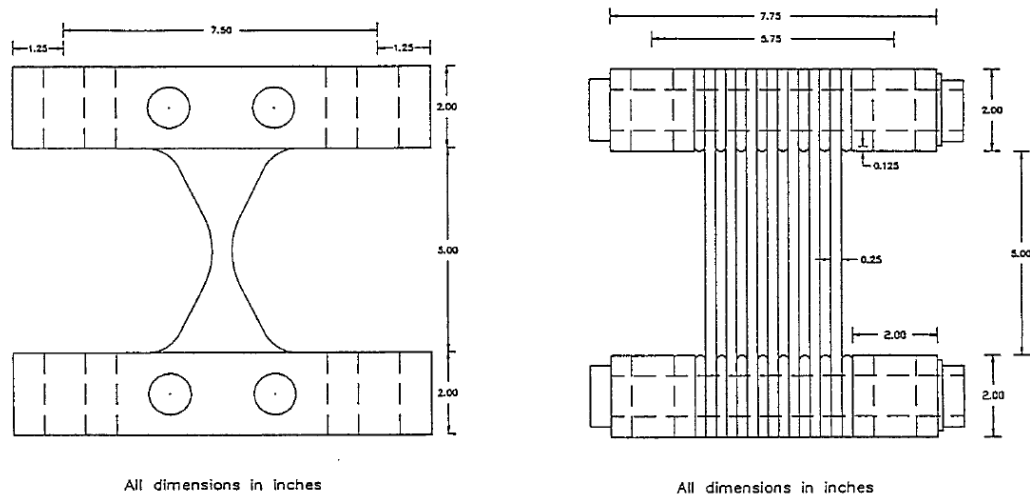


Figure 1.9: Added Damping and Stiffness (ADAS) dissipator [9]

The behaviour and the properties of the BRB will be defined in detail in the following section.

1.2.2 Key issues in conventional Buckling Restrained Braces

Horizontal acceleration from earthquakes generates horizontal inertial forces in a structure. These forces produce a lateral displacement of the building and relative displacements between consecutive floors called inter-story drift, Fig. 1.10. Inter-story drift is the principle culprit of the damage in structural and non-structural elements. For this reason restricting this movement is the way to minimize earthquake effects on the structure. So inter-story drift is one of the main design parameters of the BRB. Other key parameters are the yielding and maximum forces. These values have to be determined as a function of the weight of the structure and its dynamic properties[32].

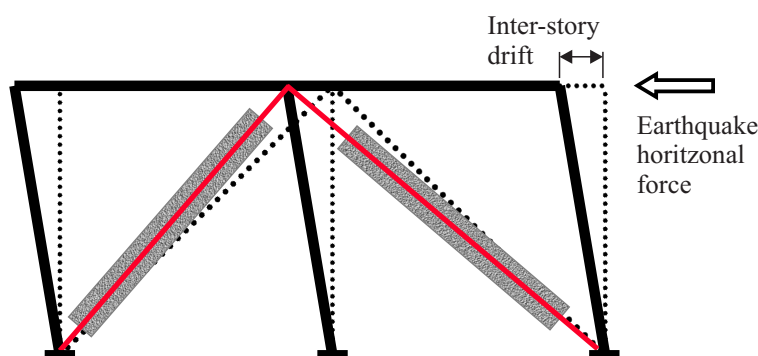


Figure 1.10: Scheme of the installation of Buckling Restrained Braces and the concept of inter-story drift

The BRBs are dissipative diagonals; the typical installation of a BRB is shown in Fig. 1.10. Under this disposition the inter-story drift causes axial strains in the BRB, these strains activate the dissipative function of the brace. BRBs are hysteresis-damping members, which absorb the seismic energy through the yielding of their metallic core (in red in Fig. 1.10), both under traction and compression axial loads. Braces are designed to yield to the earthquake design, keeping the frame in the elastic range or within acceptable damage tolerance. After the earthquake, the damaged BRBs can be replaced if its necessary.

BRB are able to work under hysteretic cycles as the earthquake causes a back and forth motion. Brace force and displacement requirements mean a slender yielding core which, when it works under compression actions, is vulnerable to second order effects such as buckling. A slender bar response under compression would be unsymmetrical with stiffness degradation (see Fig. 1.11 discontinuous pointed red line). Minimizing the buckling effects with a restraining unit, the BRB is able to dissipate a large amount of energy and the response of the brace will be mostly symmetrical (Fig. 1.11 continuous green line).

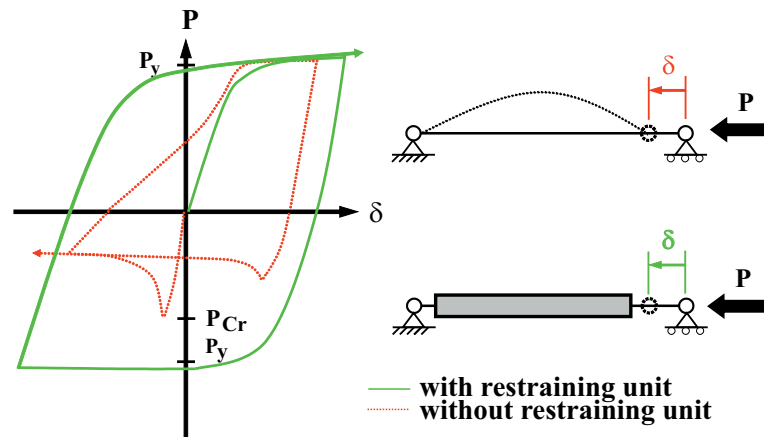


Figure 1.11: Hysteretical response of non buckling restrained frame and buckling restrained frame

For this reason, one of the most important design issues is how to avoid the buckling of the yielding core. The solution consists of using an encasing member with enough flexural stiffness to avoid global buckling and which restrains the out-of-plane displacements of the yielding core. In conventional BRBs the encasing member is composed of a steel tube filled with mortar in order to achieve dimensional compatibility Fig. 1.12. To avoid the interaction (transmission of axial forces) between the mortar and the yielding core and to allow the expansion of the core under compression forces a layer of debonding material between the core and the mortar is necessary.

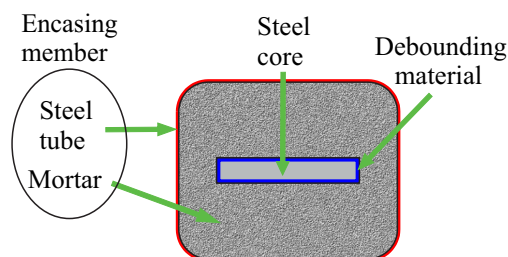


Figure 1.12: Scheme of the transversal section of a conventional Buckling Restrained Brace

1.3 Non-conventional Buckling Restrained Braces

The main shortcoming of a conventional BRB is the use of mortar to achieve the dimensional compatibility between the yielding core and the encasing member. It

causes heavy weight elements, a complex manufacturing process mainly because the use of a debonding material, and the core cannot be inspected after be damaged and substituted if necessary. Several alternatives of non-conventional BRBs have been studied and published. Chapters 2 and 3 contain short reviews about conventional and non-conventional BRBs. These chapters also contain a description of designing, testing and modelling of two innovative all-steel BRBs. In both non-conventional BRBs, the restraining unit is manufactured with several steel bars which are welded to form a hollow element providing a guiding element to the core. The debonding material is replaced by an air gap and a greased layer between the steel faces.

In Chapter 2 a new non-conventional Modular Buckling Restrained Brace (MBRB) is described. The main difference between this and conventional BRBs is that in the MBRB the dissipation of energy occurs when the steel yields under shear deformations. In Chapter 3 another new all-steel buckling restraining brace, the Slotted Buckling Restrained Brace (SBRB), is presented. As with conventional BRBs, this brace dissipates energy under axial deformation. However, the yielding does not occur along the section, but rather it takes place on the periphery of the core, which is stabilized by the rest of the core and a steel slotted encasing member. This design allows to solve the main shortcoming of the MBRB, a heavier weight when compared with conventional BRBs.

1.4 Modelling buckling restrained braces

Nowadays experimental tests are the most reliable and the most commonly used method to verify the seismic code requirements of BRBs installed to protect buildings. Full scale tests are expensive and involve a lot of work. Numerical modelling of BRBs would be a more economic option to obtain the properties of BRBs. Today, with the finite element method (FEM) software and computational capacity available, entire braces and the interaction between their elements (the core and the restraining unit) can be simulated. Having said this, modelling BRBs is challenging as the steel core of the BRB has high plastic deformations, and is submitted to low fatigue cycle phenomena which consists in low frequency cycles with high amplitude that involves plastic deformation. This is the typical behaviour that BRBs have under seismic actions. For this reason, the material models available on FEM software (such as ABAQUS [7]) to simulate the steel

behaviour are not able to properly reproduce the BRBs' experimental behaviour.

Chapter 4 contains the description, formulation and implementation in ABAQUS [7] of a constitutive model for the steel core of all-steel BRBs. Plastic behaviour is defined using a combination of isotropic and kinematic hardening, the portion of each one evolving with the amount of plastic flow. Damage is modelled using an existing model based on continuum damage mechanisms and is introduced as a post-process variable. The response of this model is compared to the experimental behaviour of the MBRB (Chapter 2).

1.5 Objectives

The main objective of this thesis is to study alternatives to conventional Buckling Restraining Braces. The greatest shortcoming of these elements is the use of mortar to achieve dimensional compatibility between the restraining unit and the yielding core. The use of mortar supposes several drawbacks: conventional BRBs are heavy weight elements, they have a complex manufacturing process, mainly because of the use of a debonding material, and their core cannot be inspected, and substituted if necessary, after sustaining damage. Also conventional BRBs with mortar and debonding material are more difficult to simulate because they have to deal with the mortar cracking and the interaction with the debonding layer. Therefore all-steel BRBs could well be an option to overcome these shortcomings. For this reason the objectives of this work can be summarized as:

- Study different options of all-steel BRBs.
- Propose analytical expressions to design the brace and the encasing member.
- Test experimental specimens to validate analytical design expressions and the proposed numerical models.
- Develop the tools to make virtual tests of the all-steel BRBs using finite element method which provides reliable results.

Chapter 2

A new modular buckling
restrained brace for seismic
resistant buildings

This chapter contains the transcription of the published paper:

Daniel Piedrafita; Xavier Cahis; Enric Simon; Jordi Comas. *A new modular buckling restrained brace for seismic resistant buildings*. *Engineering Structures* 2013; 56; 1967-1975

ISSN: 0141-0296

doi: 10.1016/j.engstruct.2013.08.013

Impact index 1,713. Journal 18 of 122, 1st quartile, Category: Engineering, Civil

The paper in journal format is shown in Appendix A

Abstract

This paper proposes a new energy dissipation device, consisting of an innovative Buckling Restrained Brace (BRB), for earthquake resistant buildings. Its steel yielding core is modular. It is based on the connection of several Seriated Modules which are comprised by an equal number of Shear Basic Dissipation units. This modular design allows adjusting the yielding force and the plastic deformation according to the building requirements. Deformation is proportional to the number of Seriated Modules and force to the number of Shear Basic Dissipation Units (on the Seriated Modules). The assembly of the brace consists in sliding the greased yielding core into the restraining unit and coupling it by pin connections. This design provides easy inspection or replacement of the dissipation unit if required. Fully-scaled prototypes have been tested under reversal cyclic displacements and the hysteretic response has been proved stable and with a high cumulative ductility. Its main parameters are the yielding force, the yielding displacement and the ultimate force; they can be predicted with simple expressions. A methodology to design the restraining unit in front of buckling is proposed, taking account the initial sway deformation and the functional gap between the yielding core and the restraining unit. The hysteretic behavior has been simulated with conventional FEM software.

2.1 Notations

A : cross-section area	n_{SBDU} : number of Shear Basic Dissipation Unit
A_v : shear area of the Basic Dissipation Unit displacement	n_{SM} : number of Seriated Modules
c : tabulated coefficient for obtaining equivalent inertia	SBDU: Shear Basic Dissipation Unit
$C_{B,max}$: maximum brace compression force	SM: Seriated Module
E : elastic modulus	$T_{B,max}$: maximum brace tension force
E_t^* : brace normalized energy	v : non dimensional coefficient for equivalent inertia on a variable cross-section member
E_t : brace hysteretic energy	W_{el} : elastic section modulus
F_B : brace force	β : non dimensional coefficient for local buckling of Shear Basic Dissipation Unit
$F_{B,cr}$: Euler buckling force of the brace	η : second order effects amplification factor
F_{By} : yielding brace force	$\Delta_{B,cum}$: cumulated brace displacement
F_f : friction force	$\Delta_{B,max}$: maximum brace displacement
F_{SBDU} : force of Shear Basic Dissipation Unit	$\Delta_{B,u}$: Ultimate brace deformation
f_u : ultimate stress	$\Delta_{B,y}$: yielding brace displacement
f_y : yielding stress	$\Delta_{SBDU,b}$: Shear Basic Dissipation Unit buckling displacement
f_{yd} : design yielding stress	$\Delta_{SBDU,y}$: Shear Basic Dissipation Unit yielding
G : shear modulus	ϵ_y : yielding deformation
I : inertia	ϵ_u : ultimate deformation
I_B : equivalent inertia for a variable cross-section member	$\gamma_{m,b}$: local buckling angular deformation
K_s : non dimensional coefficient for local buckling of Shear Basic Dissipation Unit	μ_{cum}^* : normalized cumulative
MBRB: Modular Buckling Restrained Brace	
M_m : maximum bending moment at half length of the restraining unit	

plastic deformation	ψ : non dimensional coefficient for ultimate Shear Basic Dissipation
μ_{SBDU} : Shear Basic Dissipation Unit ductility	Unit force adjustment
$\mu_{SBDU,cum}$: cumulated Shear Basic Dissipation Unit ductility	ξ : non dimensional coefficient for ultimate brace displacement

2.2 Introduction: Buckling Restrained Braces

Buckling Restrained Braces (BRBs) are elastoplastic energy dissipators used to control lateral deformation of buildings and to limit the damage under seismic loads. BRBs dissipate most of the seismic energy input via a slender restrained buckling bar yielding when submitted to reversal axial loading. A conventional BRB has an internal metallic yielding core, an outer restraining tube to prevent the flexural buckling of the yielding core, and end connections to install the brace in the building (Fig. 2.1).

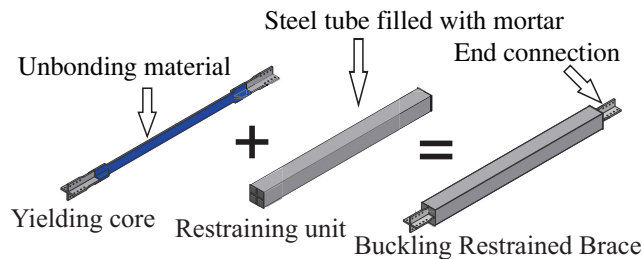


Figure 2.1: Schematic description of the conventional BRB

The dissipation core can be designed with different cross section shapes, with the most typical are rectangular, circular and cruciform [11, 24, 36, 49, 52]. The cross section of the core has to be uniform along the yielding zone to provide, under axial force, a uniform strain field. Its transverse area is sized to yield to seismic forces and its length has to be long enough to provide an adequate energy dissipation capacity. The result is a slender core that has to be restrained to avoid flexural buckling. The restraining unit is usually a steel tube manufactured from a standard profile. To remove the large clearance between the core and the restraining tube the use of mortar as filling material has become the preferred solution [25, 39, 48, 50]. Nevertheless, an operating clearance between the mortar and the yielding core is required to allow for the transverse deformation produced by the Poisson's ratio and also to avoid the transmission of the axial force

from the core to the restraining unit. This has usually been solved by adhering a layer of debonding material to the core surface. However, the use of mortar has several drawbacks. For example, the filling process makes the manufacturing more complex. In addition, the braces become heavier and this increases not only transport and installation costs, but also the seismic inertial forces. Furthermore, if the yielding core is damaged after an earthquake, the whole brace has to be replaced. Chou and Chen [21] propose a hybrid solution in the form of a sandwiched restraining unit with mortar which avoids the use of debonding material and the core can be replaced. To avoid the use of mortar, several different encasing member solutions have been proposed [10, 20, 26, 56]. Some of these solutions suggest a restraining element composed of bolted or welded profiles [10, 20, 56], while others solutions are based on the dimensional compatibility between the core and the restraining tube [26], but it is difficult to find any standard profiles which satisfy.

Sizing the restraining unit is more complex, because it depends on the flexural behaviour of a concrete-filled tube and the mortar cracking. Because of that, most researchers propose simplified expressions to design the restraining unit where mortar collaboration is basically neglected. For the restraining unit Watanabe et al. [50] propose a Euler load 1.5 times the yielding load of the core. Xie [52] describes several methods which take into account geometrical imperfections to define the bending moment to be resisted by the restraining unit. Palazzo et al. [39] improve the formulation proposed by Black et al. [11] that also considers the influence of the gap between the core and the restraining unit, the maximum compression force to design the restraining unit is obtained from the first global buckling mode. Chou and Chen [21] propose a method to design an encasing member composed of two sandwiched parts joined with bolts. They remark that the higher buckling modes have to be considered when designing the internal bolted connections of the restraining unit because these modes produce high shear forces.

This paper proposes a new Buckling Restrained Brace (BRB). Its yielding core is machined from one flat rectangular steel bar and is composed of several yielding dissipation units linked by elastic components in a modular set-up. Several simple analytic expressions for design proposes are given and contrasted with experimentally obtained data and the results from a more sophisticated numerical FEM model.

2.3 The Modular Buckling Restrained Brace.

The concept and design parameters

Over the last three decades several small devices have been designed to dissipate earthquake energy input into buildings via plastic deformation [29, 37]. These devices take advantage of the interstory drift to deform and, as they are small when compared to the story height, they have to be assembled to a laterally resistant stiff structural element, such as a reinforced concrete wall or a steel k-brace. To adapt the yielding force to building requirements, a different number of devices have to be assembled in parallel or machined from the same plate. Contrary the yielding displacement cannot be easily modified because it depends on the design of the device and its small dimensions. Buckling Restrained Braces (BRB) are larger elastoplastic energy dissipators that have solved these shortcomings, as they can directly connect different floors, and both the force and yielding deformation can easily be adjusted to the building by modifying the cross section area and length of the yielding core, respectively. On the other hand the BRBs are based on a slender yielding core submitted to axial forces and which has to be fully restrained by a metal tube usually filled with mortar. The use of mortar makes the brace heavy and complex, as well as impeding visual inspection or the replacement of the yielding core.

The Modular Buckling Restrained Brace (MBRB) was conceived from the idea of mixing the buckling self-stability of the small steel energy dissipation devices with the advantages of conventional BRBs. Like all conventional BRBs, the MBRB is composed of a slender yielding core that has to be restrained by an external tube to avoid flexural buckling, but its core is modular and it yields mainly by shear. The core (Fig. 2.2a) consists of several Shear Basic Dissipation Units (SBDUs) grouped into several Seriated Modules (SMs). The main requirement of the SBDU is to be small enough and flat enough to be compatible with the flat format of the yielding core. A shear energy dissipator [19] has been chosen but other elements, such as the honeycomb [29] or the slit damper [37], could be appropriate for the modular core of the brace. The Modular BRB (MBRB) is assembled with two yielding cores, one restraining unit and two pinned internal connections (Fig. 2.3). So the restraining tube could be further improved it has been not designed to be efficient but to be functional to test the behavior of the yielding core. It has been manufactured by welding four rectangular steel bars

together to form a tube. Two of these four bars have a milled slot and are placed facing each other to guide and stabilize the yielding cores. The brace assembly consists of pushing the greased cores into the slot of the restraining unit and fixing them in place with the internal pins. These internal pins allow the axial force from one core to the other to be transmitted by the restraining unit.

The geometry of an SM is shown in Fig. 2.2 b). The SM is provided with several paired SBDUs that have been designed to yield by shear almost uniformly along the web of the SBDU [18, 19] (Fig. 2.4). Fig. 2.15 indicates the Von Mises stress distribution and deformation of the yielding core obtained from FEM modeling. The figure shows how the plastic deformations are mostly uniform along the web of the SBDUs and how the lateral and central bands, as defined in Fig. 2.2 b), behave elastically. Fig. 2.4 shows the deformation and forces of an SBDU. Fig. 2.15 illustrates the deformation of the yielding core. It shows how the force of the brace (F_B) will depend on the force of the SBDU (F_{SBDU}) and the number of SBDUs (n_{SBDU}) in an SM, and how the ultimate plastic deformation of the brace ($\Delta_{B,u}$) depends on the deformation of an SBDU and the number of Seriated Modules (n_{SM}). Both of these design characteristics have been reflected in the following formulation.

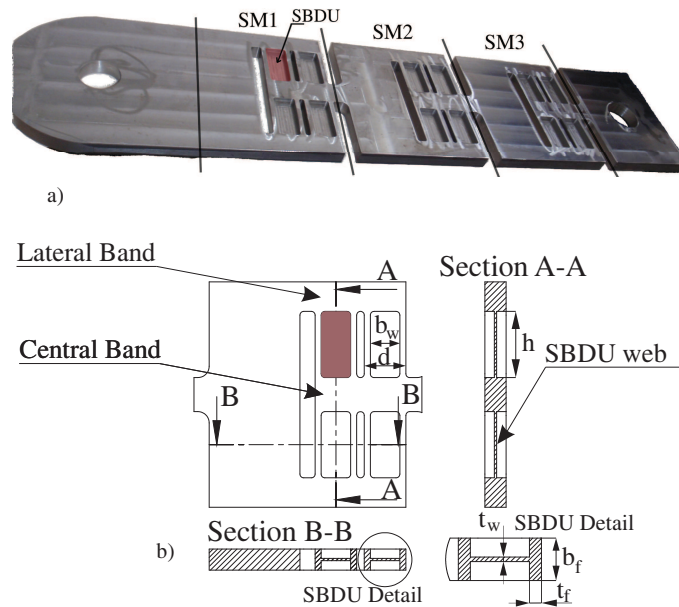


Figure 2.2: a) Modular Buckling Restrained Brace (MBRB) core geometry b) Seriated Module (SM) detail

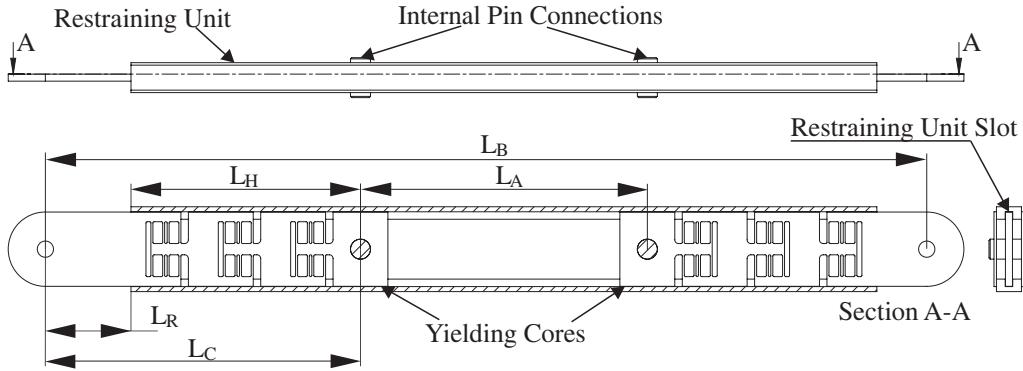


Figure 2.3: Scheme of a Modular Buckling Restrained Brace (MBRB)

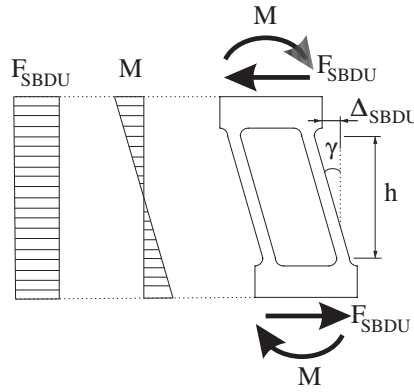


Figure 2.4: Working scheme of a Shear Basic Dissipation Unit (SBDU), internal forces distribution and shear deformation

Force of the brace (F_B) is defined as:

$$F_B = n_{SBDU} F_{SBDU} + F_f \quad (2.1)$$

as the yielding core is greased the friction force F_f can be neglected. The ultimate theoretical deformation of the brace can be determined as follows:

$$\Delta_{B,u} = \xi n_{SM} \mu_{SBDU} \Delta_{SBDU,y} \quad (2.2)$$

where ξ is a non-dimensional constant which takes into account the non-uniform plastic deformation of SBDUs caused by the non-uniformity of the web thickness because of imperfections in the milling process, n_{SM} is the number of Seriated Modules, $\Delta_{SBDU,y}$ is the yielding deformation of the SBDU and μ_{SBDU} is the ductility of the SBDU defined as the ratio between the maximum displacement and the yielding displacement.

When compared with conventional BRBs it has benefits and shortcomings. On one hand, the core has to be heavier to dissipate the same amount of energy because the linking elements behave elastically. Also, this yielding core is more complex geometrically and its manufacture is more time consuming, although it can be done by CNC machines. On the other hand, the core does not need to be restrained by mortar or concrete and covered with a debonding layer, so it can be easily assembled, inspected or changed if needed.

2.4 Design parameters of the Shear Basic Dissipation Unit

The hysteretic behaviour of the Modular Buckling Restrained Brace (MBRB) depends on the properties of the Shear Basic Dissipation Units (SBDUs). The main parameters of an SBDU are the deformations and forces at yielding and ultimate points. Based on the formulation defined by Benavent-Climent [10], the yielding force can be estimated by the following expression:

$$F_{SBDU,y} = \frac{A_v f_y}{\sqrt{3}} \quad (2.3)$$

where $A_v = dt_w$ is the shear area of the SBDU.

Ultimate force ($F_{SBDU,u}$) have been experimentally correlated (Section 2.6.3) with the ductility of SBDU (μ_{SBDU}) and the expression is defined as:

$$F_{SBDU,u} = F_{SBDU,y} (1 + \psi \mu_{SBDU}) \quad (2.4)$$

The yielding displacement can be obtained from the uniform shear strain assumption and the Navier-Bernoulli hypothesis:

$$\Delta_{SBDU,y} = \left(\frac{h^3}{12EI} + \frac{h}{\frac{5}{6}A_v G} \right) F_{SBDU,y} \quad (2.5)$$

where h is the length of the SBDU's web (Fig. 2.2 b)), E is the elastic Young modulus, I is the moment of inertia in the SBDU cross section and G is the shear modulus.

From Eq. (2.2) and Eq. (2.5) the ultimate displacement of the brace can be determined when a proper value of ductility (μ_{SBDU}) is used. Nevertheless, local buckling of the SBDU's web would significantly reduce the energy dissipation

capacity of the SBDU and it has to be avoided. Kasai [27] proposed an expression to determine the local buckling angular deformation ($\gamma_{m,b}$) for an I-beam cross-section submitted to plastic shear deformation and cyclic loads:

$$\gamma_{m,b} = 8.7K_s \frac{1}{\beta^2} \quad (2.6)$$

where $\beta = \frac{b_w}{t_w}$ and $\alpha = \frac{h}{b_w}$ (Fig. 2.2). Constant K_s depends on the parameter α and the clamping conditions of the plate [13]. Previous tests and modeling have demonstrated that the rotation of all the SBDU's web borders is nearly nil [18]. Under these conditions, $K_s = 8.98\alpha + \frac{5.6}{\alpha}$ for $\alpha < 1$ and $K_s = 5.6\alpha + \frac{8.98}{\alpha}$ for $\alpha > 1$. γ_m is defined as the difference between actual angular deformation γ and the minimum value previously reached, as shown in Fig. 2.5 [27].

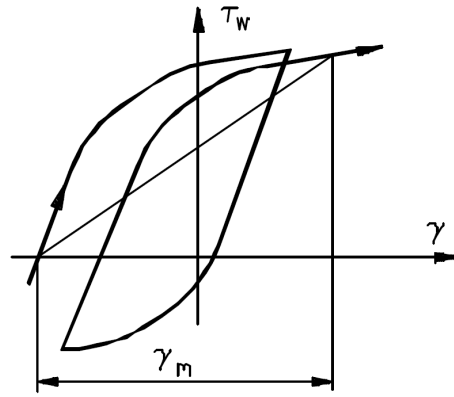


Figure 2.5: γ_m definition, Cahís [18]

Considering that the shear strain is uniformly distributed over the entire web of the SBDU [18], the angular deformation γ (Fig. 2.4) can be estimated as $\gamma \approx \Delta_{SBDU}/h$. When negative and positive maximum deformations are nearly the same (as can be assumed in seismic conditions) the local buckling displacement of the SBDU becomes:

$$\Delta_{SBDU,b} \approx 0,5\gamma_{m,b}h \quad (2.7)$$

2.5 Restraining tube design

In designing the encasing member, the functional gap between the cores and the encasing member (d_{FG}) and the initial deflection of the restraining unit at

the mid-length (e_0) (Fig. 2.6), have been considered. For the sake of simplicity and security, the restraining of rotation by the pin connection in the z -axis has been neglected, so the following formulation is valid for both flexural planes of the restraining unit. Only the first mode is considered because the influence of higher modes can be neglected [39].

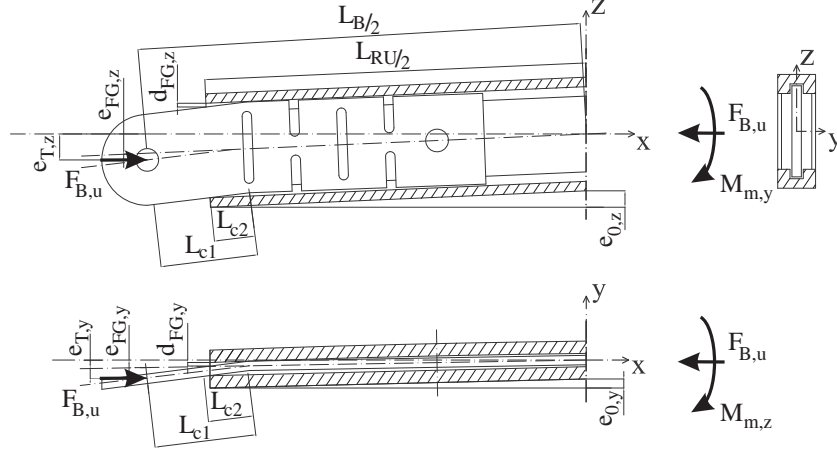


Figure 2.6: Effects of the geometrical imperfections on the end connections

The initial eccentricity e_{FG} produced because of the functional gap d_{FG} can be obtained as:

$$e_{FG} = \frac{d_{FG}}{L_{c2}} L_{c1} \quad (2.8)$$

The combined effect of the initial imperfection and the functional gap results in the total eccentricity:

$$e_T = e_0 + e_{FG} \quad (2.9)$$

The maximum bending moment at the half length of the restraining unit (Fig. 2.6) can be expressed as:

$$M_m = \eta F_{B,u} e_T \quad (2.10)$$

where η is the amplification factor [3] that takes into account second order effects:

$$\eta = \frac{1}{1 - \frac{1}{\alpha_{cr}}} \quad (2.11)$$

where $\alpha_{cr} = \frac{F_{B,cr}}{F_{B,u}}$, and $F_{B,cr}$ is the Euler buckling force for a bar with a variable cross section:

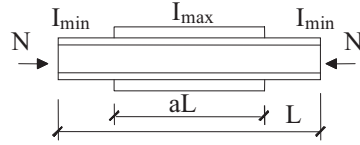


Figure 2.7: Idealized variable cross-section bar [4]

$$F_{B,cr} = \frac{\pi^2 EI_B}{L_B^2} \quad (2.12)$$

I_B is the equivalent moment of inertia of the MBRB, that can be obtained when considering the brace as a member of the variable cross-section bar with a constant axial load Fig. 2.7. CTE [4] propose a method using equivalent inertia:

$$I_B = cI_{max} \quad (2.13)$$

c is obtained using tabular data defined by values of a (Fig. 2.7) and v :

$$v = \sqrt{\frac{I_{min}}{I_{max}}} \quad (2.14)$$

The I_{min} is the moment of inertia of the yielding core cross section, the I_{max} is the moment of inertia of the restraining unit and aL is the length of the restraining unit. These assumptions can be justified from Fig. 2.6, which shows that the contribution of the core to the brace bending stiffness is limited to the outside of the restraining unit, because the internal part of the core, which has been milled, is too flexible to be considered.

The resistance of the restraining unit can be checked by combining the flexural moments in both axes with the axial force. When considering elastic behavior the check is (class 3 section [3]):

$$\frac{M_{m,y}}{W_{el,y}f_{yd}} + \frac{M_{m,z}}{W_{el,z}f_{yd}} + \frac{F_{B,u}}{Af_{yd}} \leq 1 \quad (2.15)$$

where W_{el} is the elastic section modulus, A is the cross-section area of the restraining unit and f_{yd} the design yield strength ($f_{yd} = \frac{f_y}{1.05}$).

2.6 Experimental behavior

2.6.1 Test set-up and push protocols

The tests were performed in the structural laboratory of the AMADE research group of the University of Girona (Spain). Fig. 2.8 shows the test set-up, based on a brace-column subassembly proposed by the AISC341-05[2]. The Modular Buckling Restrained Brace (MBRB) specimens were fixed to the structural slab and to a column by two pinned connections (Fig. 2.8). A 300 kN servo-controlled hydraulic actuator fixed to the reaction frame was used to load the subassembly. Three specimens were tested under different test protocols, until failure was reached (Fig.2.9). The maximum MBRB deformation for the AISC341-05[2] and EN15129[5] protocols was calculated considering a 3 m high story and one percent of the interstory drift as a seismic design displacement. Only one of the cores was designed to yield, because two yielding cores would not provide additional relevant information. Because of this, the maximum displacement used for both the AISC341-05[[2] and the EN15129[2] protocols was reduced to half of that corresponding to a full Modular Buckling Restrained Brace (a MBRB with two yielding cores). The deformation of the whole brace was obtained by the sum of the deformation of the brace displacement transducers B1 and B2. (Fig. 2.8). Transducer B1 measures the relative displacement between the external upper pinned connection and the lower end of the restraining unit, while transducer B2 measures the displacement between the bottom end of the restraining unit and the bottom external pinned connection. Thus, transducer B2 measured the deformation of the yielding core. The deformations of the Seriated Modules were obtained from transducers SM1, SM2 and SM3 (Fig. 2.10).

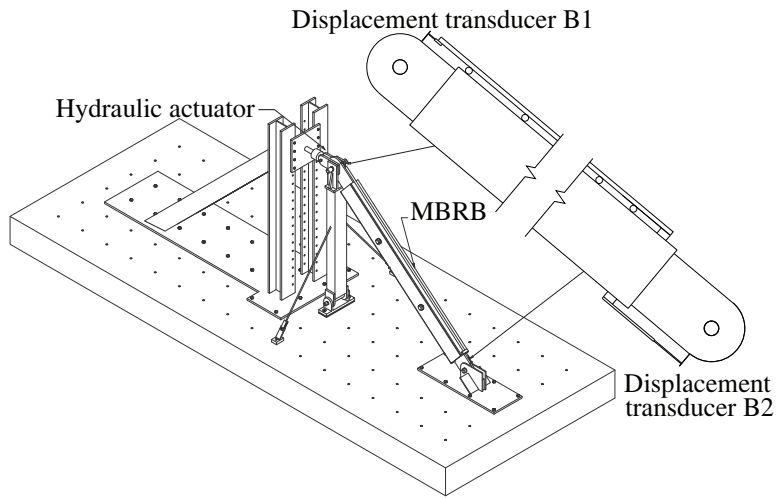


Figure 2.8: Scheme of test set-up

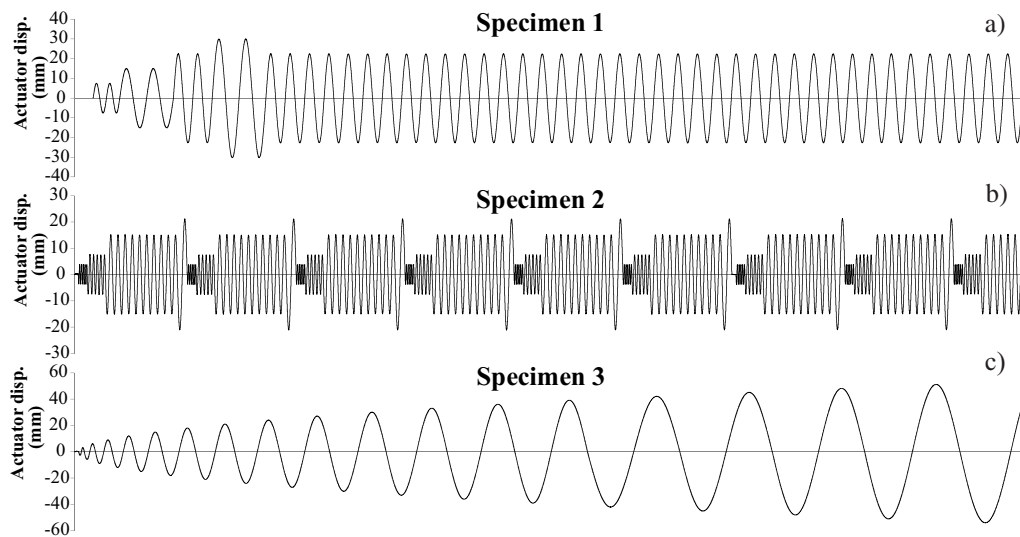


Figure 2.9: Push protocols: a) AISC341-05[2] protocol b) EN15129[5] protocol c) Cyclic deformation with increasing amplitude

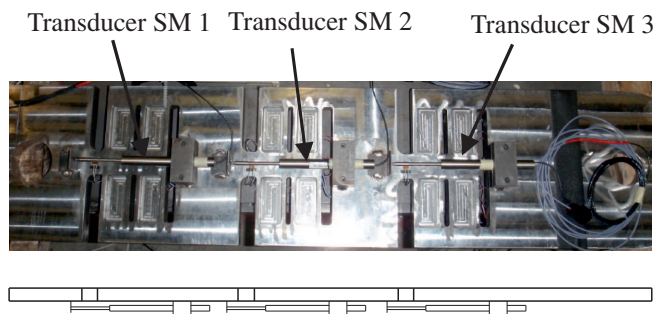


Figure 2.10: Core transducers localization

2.6.2 Tested specimens

Steel S275JR [1] was used to manufacture both the yielding cores and the restraining tube. The mechanical properties of the steel of the yielding cores were determined by a tension test [19]: $f_y=279$ MPa; $\epsilon_y=0.14$ %; $f_u=434$ MPa; $\epsilon_u=21$ %. The main dimensions of the tested specimens were $L_B=3533$ mm; $L_A=1150$ mm; $L_C=1120$ mm and $L_R=343$ mm (Fig. 2.3). As for the geometry of the cores, the main parameters were $d=55$ mm, $h=87.5$ mm, $b_w=39$ mm, $b_f=28$ mm and $t_f=8$ mm (Fig. 2.2 b)). It was anticipated that small differences in the thickness of the webs of the Shear Basic Dissipation Units (t_w) could cause significant differences of deformation in the SMs, so this parameter was carefully measured with a Computer Numerical Control Coordinate Measuring Machine. Table 2.1 shows the averaged thicknesses for each SBDU web.

Average thickness			
[mm]	SP1	SP2	SP3
SM1	2.86	2.50	2.67
SM2	2.64	2.53	2.78
SM3	2.96	2.55	2.80

Table 2.1: Average thickness of Shear Basic Dissipation Units (SBDUs) (t_w)

2.6.3 Experimental results

Fig. 2.11 shows the total deformation of the cores versus the force of the brace until failure. The SBDUs did not suffer local buckling. A stable and symmetric hysteretic response was obtained from all specimens tested.

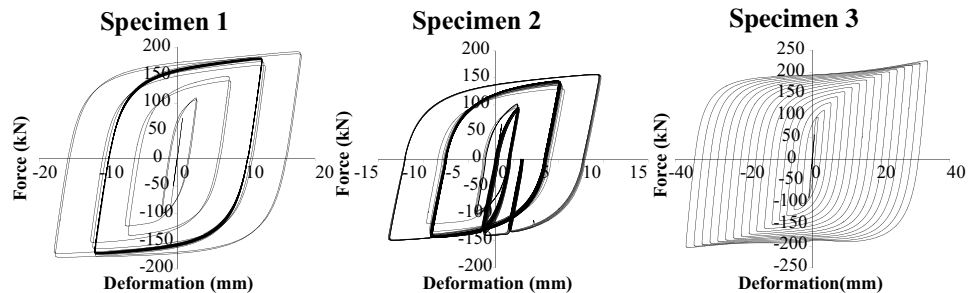


Figure 2.11: Force versus total deformation of each specimen core

Fig. 2.12 shows the response of each Seriated Module (SM). We can observe how all the modules have a stable response and significant yielding deformation, and can confirm that the SM with the lowest average thickness (Table 2.1), has the larger deformation and the maximum cumulative deformation, causing brace failure. This effect was more evident in specimen 1 (Fig. 2.12 a)), where SM 2 had the lowest web thickness of the SBDU and concentrated most of the deformation. The plastic deformation of the Modular Buckling Restrained Brace (MBRB) became more uniform when the thickness of the SBDUs was also more uniform.

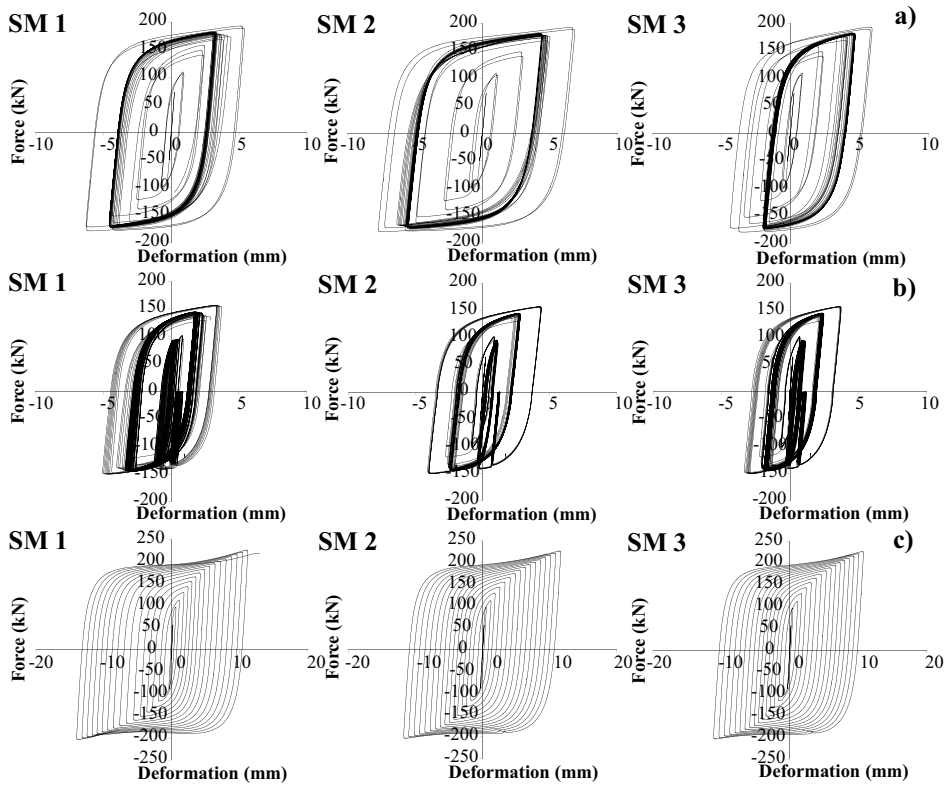


Figure 2.12: Experimental response of each Seriated Module (SM) a) Specimen 1 b) Specimen 2 c) Specimen 3

Table 2.2 summarizes the experimental results for all specimens. $T_{B,max}$ and $C_{B,max}$ are the maximum tension and compression forces, respectively. $\Delta_{B,max}$ is the maximum deformation, $\Delta_{B,cum}$ is the cumulated plastic deformation of the brace. μ_{SBDU} is the ratio $(\frac{\Delta_{SBDU,u}}{\Delta_{SBSU,y}})$ where $\Delta_{SBDU,u}$ is the maximum experimental displacement of the SBDU (obtained by considering as non-significant the elastic deformation of the Seriated Module (SM) at maximum displacement)

and $\Delta_{SBDU,y}$ is the value obtained using Eq. (2.5). $\mu_{SBDU,cum}$ is the relationship $(\frac{\Delta_{SBDU,cum}}{\Delta_{SBDU,y}})$. E_t is the hysteretic energy of the brace.

	Sp 1	Sp 2	Sp 3
$F_{B,y}$ (kN)	90	88	88
$\Delta_{B,y}$ (mm)	1.15	1.25	1.41
$T_{B,max}$ (kN)	192.9	156.8	226.5
$C_{B,max}$ (kN)	178.8	149.82	203.0
$F_{B,max}/F_{B,y}$	2.15	1.78	2.57
$T_{B,max}/C_{B,max}$	1.09	1.18	1.12
$\Delta_{B,max}$ (mm)	18.87	13.06	37.72
$\Delta_{B,cum}$ (mm)	1282.86	2795.32	1130
μ_{SBDU}	45.2	29.7	82.4
$\mu_{SBDU,cum}$	4876	5654	2436
E_t (kJ)	281	287	203

Table 2.2: Summary of experimental results

The linear regression obtained representing ultimate brace deformation versus ultimate SBDU deformation provides, according to Eq. (2.2), an experimental value of $\xi = 0.9$.

Ultimate force ($F_{SBDU,u}$) has been linearly correlated with ductility (Fig. 2.13) and to make the correlation average yielding force has been added to the experimental ultimate forces. According to Eq. (2.4), an experimental value of $\psi = 0.0133$ has been obtained.

From low-cycle fatigue a linear relationship between the ductility and the cumulative ductility can be appreciated from Fig 2.14. As Eq. (2.2) shows, the ductility of the SBDU is a fundamental design parameter in obtaining the

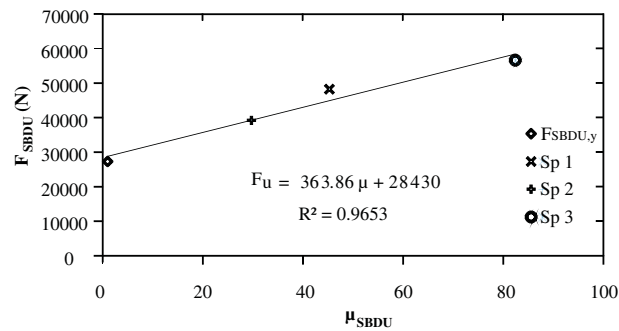


Figure 2.13: Linear correlation between the ultimate force ($F_{SBDU,u}$) and Shear Basic Dissipation Unit ductility (μ_{SBDU})

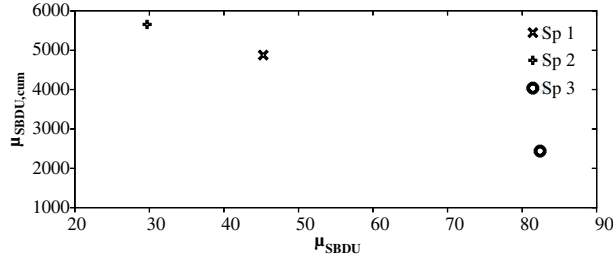


Figure 2.14: Cumulated Shear Basic Dissipation Unit Ductility ($\mu_{SBDU,cum}$) vs. Shear Basic Dissipation Unit Ductility (μ_{SBDU})

minimum number of SMs which satisfy the maximum deformation. From the push protocols AISC341-05[2] and EN15129[5] experimental ductilities of 30 and 45 have been obtained, respectively.

The hysteretic responses of specimen 1 and a conventional BRB [36] tested under similar push protocols have been compared (table 2.3). The comparison includes the hysteretic energy and the cumulative deformation, which have been normalized respectively as $E_t^* = \frac{E_t}{F_{B,y}\Delta_{B,y}}$ and $\mu_{cum}^* = \sum (\frac{2(\Delta_i^+ + \Delta_i^-)}{\Delta_y} - 4)$, and the ratio between the maximum tension and compression forces. Unlike conventional BRBs, the MBRB has a less than 1 ratio between the maximum compression force and the tension force. This demonstrates that the friction force between the restraining unit and the core (Eq. (2.1)) is very low and can be neglected. Although normalized values of the total dissipated energy and cumulative ductility are comparable, to obtain absolute similar values the core of the MBRB should be heavier because it contains parts with a linking function which behave elastically.

	E_t^*	μ_{cum}^*	$\frac{C_{max}}{T_{max}}$
MBRB	2685	1914	0.92
BRB 1 [36]	1597	1143	1.17
BRB 2 [36]	1480	1083	1.28

Table 2.3: Comparison of normalized hysteretic energy (E_t^*), normalized cumulative plastic deformation (μ_{cum}^*) and maximum tension and compression forces between a MBRB and a conventional BRB (Newell et al. [36])

2.7 Numerical prediction

The behavior of the yielding core of the Modular Buckling Restrained Brace (MBRB) has been simulated using the available commercial Finite Element (FE) software ABAQUS/Standard, version 6.9 [6].

Geometry has been modelled using S4R and S3 shell elements, because the thickness of MBRB is much lower than its other dimensions. The material constitutive model of steel has been defined using a multilinear function with combined kinematic and isotropic hardening, as defined in ABAQUS/Standard [6] (Table 2.4).

Stress (MPa)	0	279	290	402	434
Strain	0	0.0014	0.0167	0.0790	0.1699

Table 2.4: Material properties of the numerical model

According to the values given in Table 2.1, the model includes the average thickness of the web of each SBDU in specimen 1,

The pin connection has been modelled by coupling all the nodes of the hole to a virtual node created in the center of the hole. All the degrees of freedom of the hole nodes are coupled with the node in the center and in this node only the rotation around the edge hole has been allowed. The out-of-plane displacement of all the nodes on the neutral axis has been restrained to simulate the effect of the restraining unit. The model has been loaded under displacement control and a displacement (u) has been applied (Fig. 2.15).

Fig. 2.15 also shows the Von Misses stress on the core at maximum displacement. The stress on the SBDUs is uniform. As the Seriated Module 2 has the lowest average web thickness (table 2.1) its shear deformation is the highest.

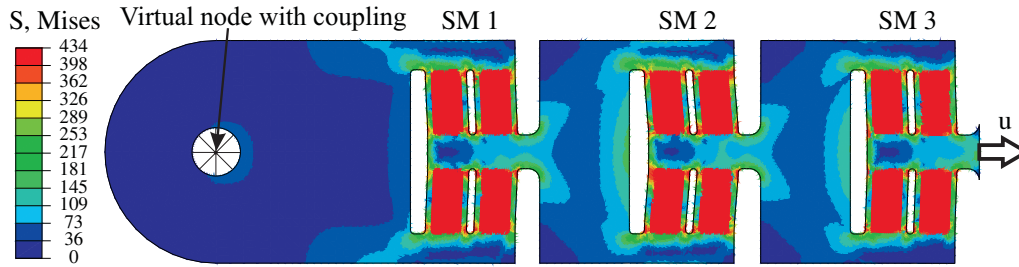


Figure 2.15: Stress distribution at maximum displacement of the FEM model, specimen 1

Fig. 2.16 compares the numerical response with the experimental response of specimen 1. The response of the numerical model is stable and symmetric and elastic and post-elastic stiffness are the same in the tension mode as in the compression mode. We can observe how the numerical model is able to reproduce the general experimental behavior of the prototype. Its yielding force and its yielding displacement agree with those obtained experimentally and with the simplified models (table 2.5)

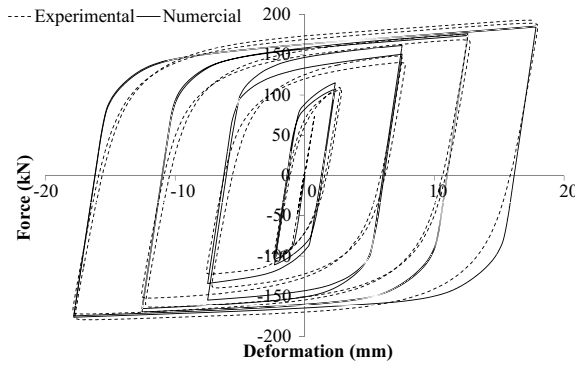


Figure 2.16: Experimental vs. numerical response

	Exp.	An.	Num.
F_{SBDU_y} (kN)	22.5	23.4	24.7
$\Delta_{SBDU,y}$ (mm)	0.25	0.20	0.22

Table 2.5: Comparison between experimental, analytical and numerical results, specimen 1

2.8 Summary and conclusions

An innovative Modular Buckling Restrained Brace (MBRB) has been designed and tested. The yielding cores are prevented from buckling by a restraining tube provided with two slots where the yielding cores slide in. Unlike conventional BRBs, the new MBRB does not need to be filled with concrete, therefore, the proposed MBRB is simpler to assemble and the yielding units can easily be inspected and substituted if they are damaged. However, as the plastic deformation is not uniformly extended, and contrary to conventional BRB, the MBRB has to be heavier than a conventional BRB to obtain the same energy dissipation capacities. The yielding cores are modular and consist of several Shear Basic Dissipation Units (SBDUs) grouped into several Seriated Modules (SMs). The axial force of the MBRB is proportional to the number of SBDUs at each SM and to SBDU force. The deformation of the MBRB is proportional to the number of SMs and to the deformation of the SBDUs.

Three specimens have been tested under different test protocols until failure was reached. The hysteretic curve of the tested specimens is stable and symmetrical. The plastic deformation of BRBs becomes more uniform over the entire brace when the thickness of the SBDUs is also more uniform. It has been experimentally confirmed that the maximum deformation and the failure of the brace always appear in the SM which has the SBDUs with the lowest average web thickness.

Several expressions have been proposed to predict the force and the deformation at the yielding and ultimate points. These expressions have been adjusted and validated using the experimental results. The ultimate parameters refer to the ductility of the SBDUs, and with values of between 30 and 50, have satisfied the requirements of the standard American and European testing protocols considered for BRBs, AISC341-05[2] and EN15129[5], respectively.

The hysteretic response of the MBRB has been compared with the response of a conventional BRB. Unlike conventional BRBs, the MBRB has a less than 1 ratio between the maximum compression force and the tension force, which shows that the friction force between the core and the restraining unit of the MBRB is non-significant. Although normalized values of the total dissipated energy and cumulative ductility are comparable, the core of the MBRB should be heavier to obtain absolute similar values because it contains parts with a linking function which behave elastically.

A methodology and several expressions for the sizing of the restraining tube have been also proposed. Bending, second order effects produced by the initial deflection of the restraining unit and the functional gap between the slots of the restraining unit and the yielding cores have been taken into account.

Finally, the hysteretic behavior of the MBRB has been numerically simulated with the commercial finite element program ABAQUS[6] and a good correlation has been found between the numerical and the experimental data.

2.9 Acknowledgements

This work was supported by the Spanish Government under Project MEC BIA2011 26816. The research groups of GREP and AMADE (University of Girona) and Bellapart Company (Olot - Spain) have collaborated in the manufacturing and testing of the specimens. Their help is gratefully acknowledged.

Chapter 3

A new slotted buckling restrained brace

This chapter contains the transcription of the submitted paper:

Daniel Piedrafita; Xavier Cahis, Dr; Enric Simon; Jordi Comas. *A new slotted buckling restrained brace*. Submitted to Engineering Structures.

Impact index 1,713. Journal 18 of 122, 1st quartile, Category: Engineering, Civil

Abstact

The Slotted Buckling Restrained Brace (SBRB) is a new energy dissipation device for the seismic design of buildings. It consists of two steel plates, which work as yielding elements and which are guided and partially stabilized by a slotted restraining unit. The plates and the restraining unit are connected by two internal pins to transmit the axial force from both brace endings. The plates are mechanized to obtain two yielding lateral bands which are connected by several equidistant stabilizing bridges. The lateral bands are designed to yield to axial forces, as conventional BRBs do, so the force and the displacement at the yielding point can be calculated by the usual expressions of conventional buckling restrained braces, based on uniform strain distribution. To distribute the stabilizing bridges along the core, an expression based on Euler's formulation is proposed. Under this formulation two types of specimens have been designed and tested (Type I and Type II) using three different loading protocols. The Type I specimens exhibited a stable response, while the Type II specimens suffered a progressive loss of compression capacity produced by the local buckling. Finally, the hysteretic behaviour of the tested braces has been analysed with an FEM model which considers the interaction between the core and the encasing member. The model reproduces the hysteretic response during the first cycles and the influence of friction on the axial strain distribution along the yielding core.

3.1 Introduction

Passive energy dissipation devices are a widely accepted solution used to improve the response of the structures under seismic conditions [45]. One of the most widespread energy dissipation devices is the Buckling Restrained Brace (BRB). BRBs can be installed like a conventional concentric brace to control the lateral interstory drift. They basically consist of a slender bar, which acts as the axial-resistant component designed to yield and to dissipate energy, and an encasing member to keep the bar stable under compression forces [50].

In order to achieve a uniform strain field under tension and compression, the cross-section core of conventional BRBs is uniform. The most commonly used cross sections are either rectangular, circular or cruciform [11, 24, 36, 49, 52]. The restraining member is usually based on a tubular profile filled with mortar [12, 49] (Fig.3.1). In this case a debonding material has to be applied to the core to enable its free lateral expansion under compression, and to keep the transmission of the axial force from the core to the restraining unit low [48]. It is a very effective solution which gives a stable hysteric behaviour however, it increases the weight of the brace and makes a visual inspection of the core or its replacement in case of damage impossible. The use of precast concrete in steel profiles [21, 25], enables easy inspection and replacement. All-steel BRBs [20, 24, 40] avoid both the use of mortar and the debonding layer and ensure inspection and replacement by providing dimension compatibility with the use of a restraining unit composed of several parts which are either bolted or welded. Piedrafita et al. [41] propose a non-conventional BRB which yields by shear, and consists in a slender bar restrained by a slotted restraining unit. Its core is very easy to assemble and to inspect, but it is heavy and its mechanization is more complex and expensive than that the required in conventional BRBs.

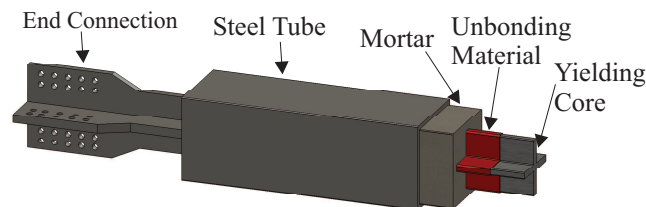


Figure 3.1: Scheme of conventional buckling restrained brace parts

A new buckling restrained brace is purposed in this paper. It yields under axial forces as a conventional BRB does, but the usual massive core has been

substituted by a partially emptied plate shaped by water jet cutting. The core is a one-piece element composed of two lateral bands, of a nearly uniform section and designed to yield, connected by stabilizing bridges, which have to remain elastic. This design enables the lateral bands to be located in two slots of a restraining unit. These two slots and the stabilizing bridges enable the lateral band yield to be restrained and stable. Design expressions have been proposed and experimental tests have been carried out. Finally, a numerical model has been made to study the interaction between the core and the encasing member and the effects of friction in the strain distribution on the lateral bands.

3.2 Slotted buckling restrained brace

The yielding core of BRBs usually consists of a solid slender bar. To avoid buckling under compression forces, the entire surface of the core has to be close to the internal surface of the restraining unit. This has been solved in various ways, such as filling the clearance between the core and a standard steel tube with mortar (Fig.3.2 a) and b)), or assembling standard bars around the core (Fig.3.2 c)). The new Slotted Buckling Restrained Brace (SBRB) has a partially emptied flat core to locate the entire yielding cross section in the periphery of the brace; away from the brace axis (Fig.3.2 d)). It is made of two steel plates (the yielding cores), which are guided and partially stabilized by the internal slots of a steel restraining unit (Fig.3.3). To transmit the axial forces from both external brace connections, the cores and the restraining unit are connected by internal pins. The core, which consists of a partially emptied plate shaped so that the two lateral bands are connected by equidistant transverse stabilizing bridges (Fig.3.4), is machined with a water jet cutter to avoid causing any changes to the mechanical properties of the material. The lateral bands are designed to yield to axial forces, as with conventional BRBs, while the stabilizing bridges are designed to remain elastic. The stabilizing bridges, along with the slots in the restraining unit, keep the lateral bands stable under compression. The restraining member has been manufactured by welding four rectangular steel bars together to form a tube. Two of these four bars have a milled slot and are placed facing each other to guide and stabilize the yielding cores. The brace assembly consists of pushing the greased cores into the slot of the restraining unit and fixing them in place with the internal pins.

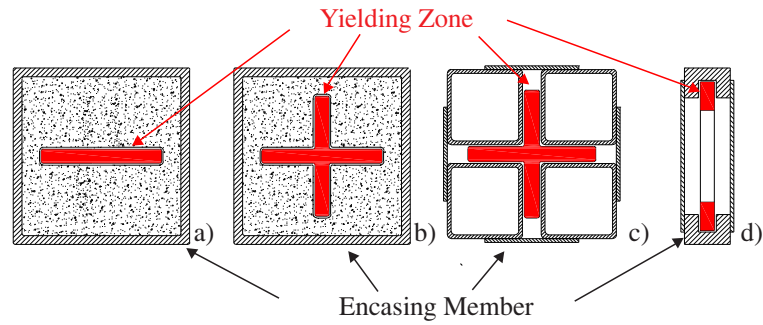


Figure 3.2: a) and b) sections of conventional BRB, c) all-steel BRB and slotted buckling restrained brace d)

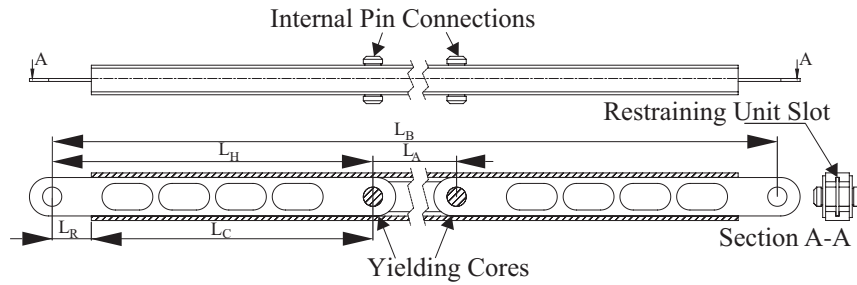


Figure 3.3: Brace assembly

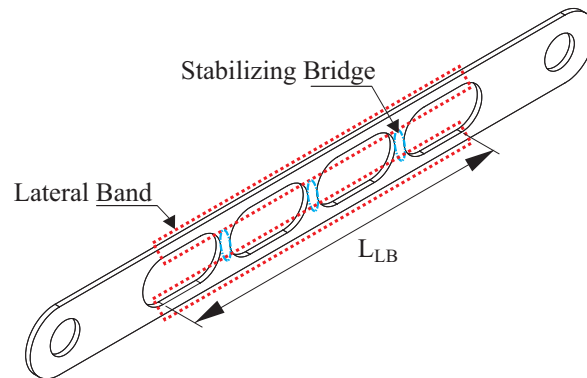


Figure 3.4: Slotted buckling restrained brace core, lateral bands in red, stabilizing bridges in blue.

The lateral band design is based on uniform stress assumption. The yielding force (F_y) and the ultimate force (F_u) of the core can be obtained by using Eq. (3.1) and Eq. (3.2), respectively:

$$F_y = 2f_y tb \quad (3.1)$$

$$F_u = 2\beta f_u t b \quad (3.2)$$

where t and b are the thickness and width of the lateral band, respectively (Fig. 3.5); f_y and f_u are the yielding and ultimate material strengths, respectively, and β is a hardening experimental factor which takes into account the compression peak caused by the interaction between the core and the restraining unit [2, 48]. The yielding deformation $\delta_{c,y}$ can be obtained from Hook's law when taking into account the Young's Modulus of the steel E :

$$\delta_{c,y} = \frac{F_y L_{LB}}{E t b} \quad (3.3)$$

where L_{LB} is the length of the lateral band (Fig. 3.4). This expression has been validated using the numerical model (Section 3.5) and the experimental results (Section 3.4).

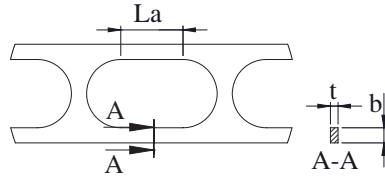


Figure 3.5: Key dimensions of the core

As the ultimate deformation is mostly plastic and it happens in the cores, the ultimate displacement of the brace ($\delta_{b,u}$) can be estimated as the addition of the ultimate deformations of the yielding cores. The ultimate deformation of the core ($\delta_{c,u}$) can be obtained by Eq. (3.4).

$$\delta_{c,u} = \mu_c \delta_{c,y} \quad (3.4)$$

where μ_c is the ductility of the yielding core. The yielding cores should be designed to a maximum ductility of 8 to deal with the design inter-story drift; as is obtained from the experimental results.

To define length L_a the premise was that on-plane local buckling does not appear. Euler formulation ($\frac{\pi^2 EI}{k L_a}$) is used, where the rotation at the ends of the yielding zones is considered nil ($k = 0.5$); as experimental results confirm. From these considerations:

$$L_a = \sqrt{\frac{\pi^2 E_t t b^3}{3F_{max}}} \quad (3.5)$$

where I is the moment of inertia of the lateral band ($I = \frac{tb^3}{12}$) and E_t is the tangential plastic modulus at maximum force on the traction test; as is proposed by Black et al. [12].

The SBRB and the Modular Buckling Restrained Brace (MBRB) [41] are very similar. In fact, the SBRB adopts the concept of the slotted encasing unit from the MBRB. The main difference between them is in the yielding core. Therefore, the same formulation as [41] is proposed to design the encasing member of the SBRB.

3.3 Test set-up and push protocols

The tests were carried out in the Structural Laboratory of the AMADE research group at the University of Girona. Fig. 3.6 shows the set-up; based on brace-column subassembly defined in the AISC341-05 [2].

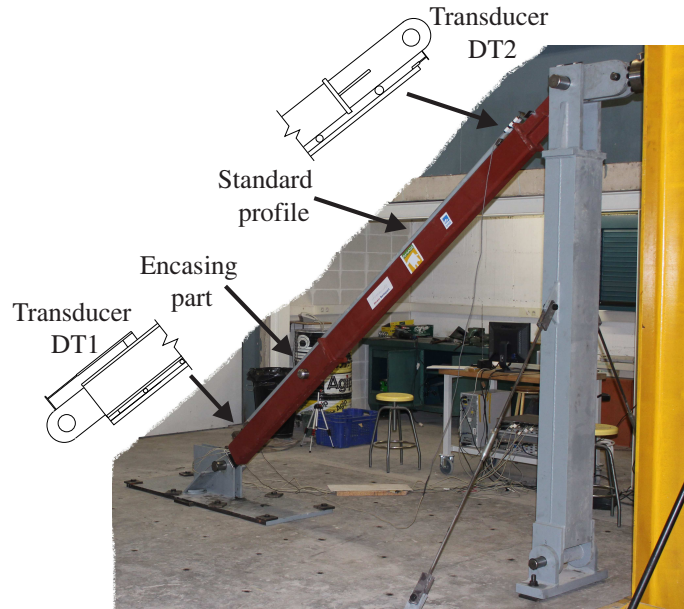


Figure 3.6: Test set-up, restraining unit parts and external displacement transducer positions

The brace was installed using pin connections. The maximum MBRB deformation for the AISC341-05 [2] and EN15129 [5] protocols was calculated for a

3 m high story with one percent inter-story drift as the seismic design displacement. Subassembly was loaded with a 300 kN servo-controlled hydraulic jack. While SBRB is designed to have two cores, one at either end, testing with one core provides the same relevant information if the design displacement is reduced to half. This set-up has the advantage of making the testing more cost-effective. With these factors in mind, braces with a single dissipation core were built and tested. Half of the brace was as Fig.3.3 shows, and the other half consisted of a standard rectangular hollow tube with an external pin connection. The hollow tube and the slotted restraining unit were welded together by a connection plate.

An internal transducer measured the core deformation (Fig.3.7). Two external transducers (DT1 and DT2, Fig.3.6) were used to measure the deformation of the brace. While DT1 measured the core and the internal pin deformations, DT2 measured the elastic deformation of the rest of the brace.

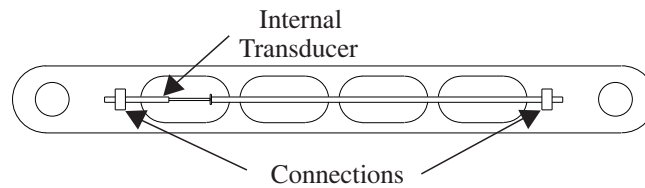


Figure 3.7: Internal transducer position

The yielding cores were manufactured using S275JR [1] steel. The mechanical properties were obtained according to tension tests defined in [3]: $f_{yk}=267$ MPa; $\epsilon_y=0.13$ %; $f_{uk}=455$ MPa; $\epsilon_u=26$ %. The cores were machined by using water jet cutting to avoid any changes in the mechanical properties because of heat. Two types of specimens were designed and manufactured (Fig.3.8). In Type I, the L_a dimension was defined by using Eq.(3.5), therefore local instability was not expected. Type II were designed beyond the length provided by Eq.(3.5). Hence early core failure, caused by local instability, was expected.

Six specimens, three of each type, were tested to failure. These specimens have been named according to their geometry (two variants, Type I and Type II) and testing protocol. The specimens I.1 and II.1 were tested under the AISC341-05 [2] protocol, specimens I.2 and II.2 were tested under EN15129 [5] and specimens I.3 and II.3 were tested using a cyclic deformation with increasing amplitude protocol. The push protocols are shown in Fig.3.9.

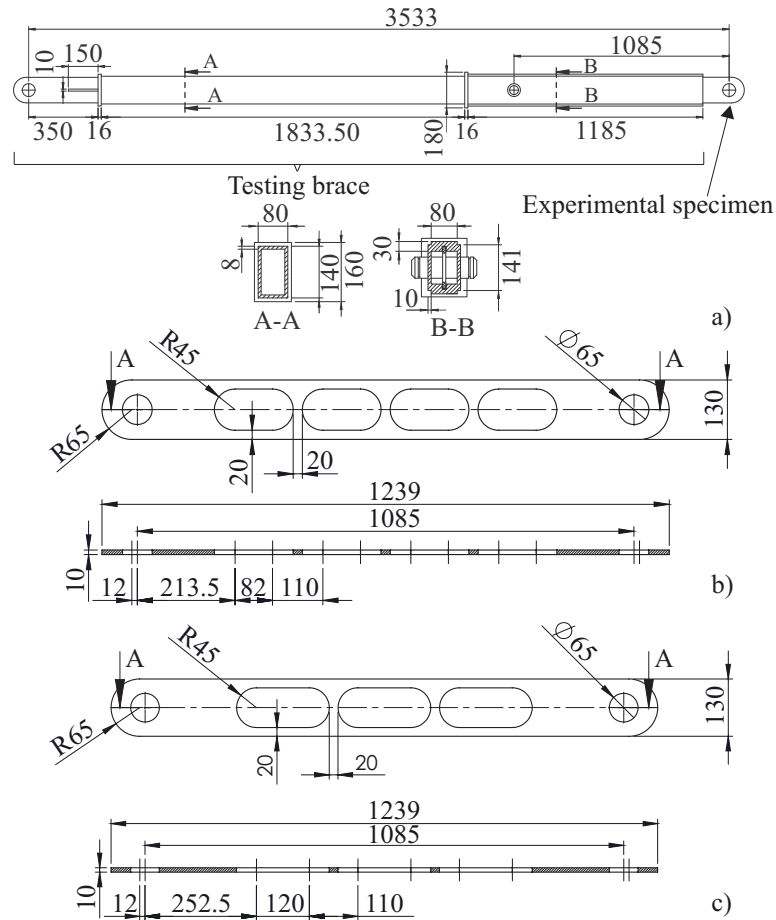


Figure 3.8: Experimental specimens: a) Type I b) Type II

3.4 Experimental results

Fig. 3.9 shows the experimental response of the specimens. Specimens II.1 and II.3 suffer a progressive loss of compression capacity. Fig. 3.10 shows the deformation of these two specimens after failure. The high deflection confirms local buckling. On the other hand, specimens I.1 and I.3 show a lower deflection and fail by tension; as the hysteric response and visual inspection indicates. They also dissipate a higher amount of energy; as illustrated by Table 3.1. These results confirm that Eq. 3.5 is suitable for designing a stable core under compression.

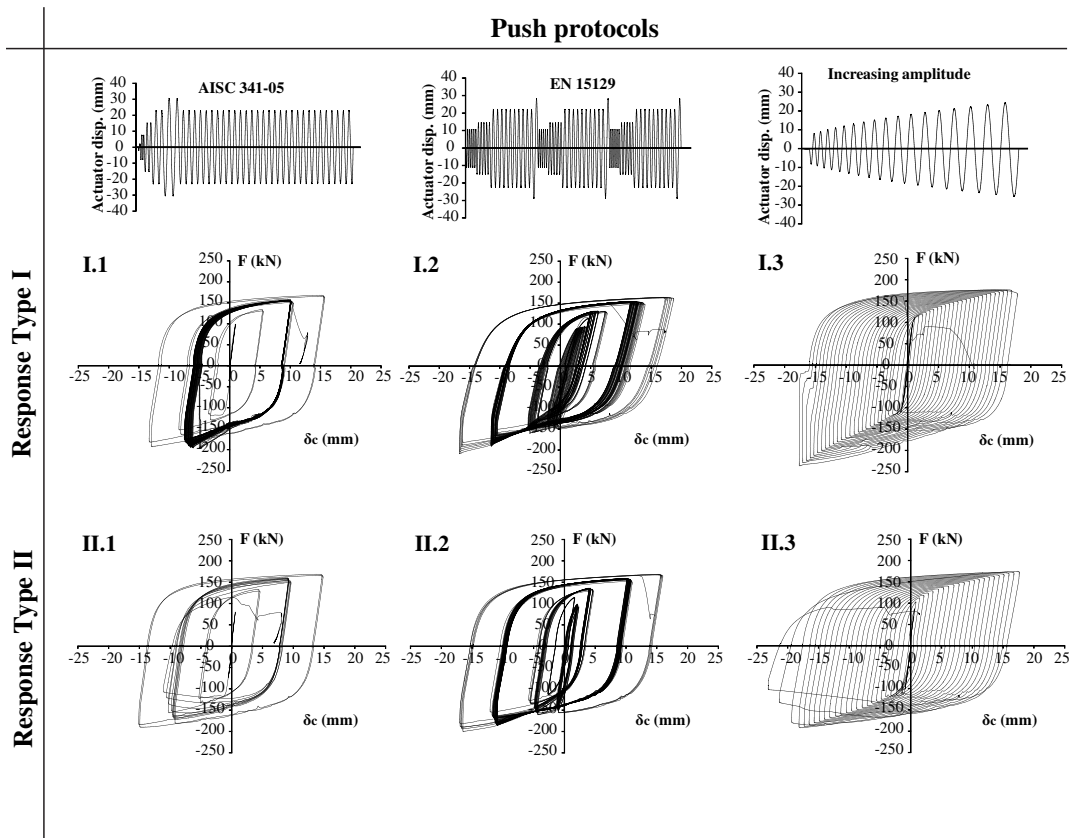


Figure 3.9: Experimental results and applied push protocols

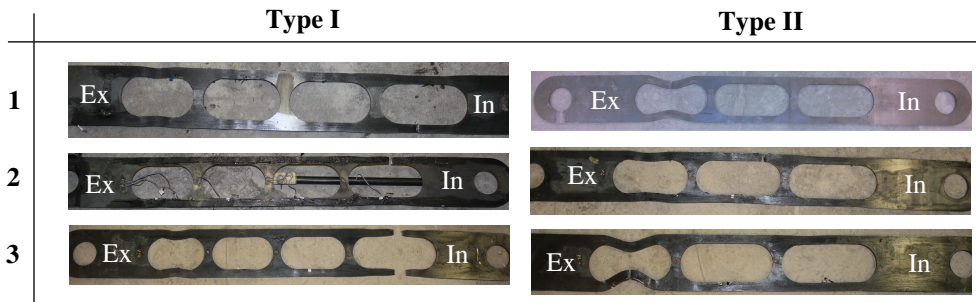


Figure 3.10: Failure mechanism of the specimens. Ex: External zone, In: Internal zone

Although local buckling appeared in two of the tested specimens, all of them satisfied the test protocols until failure. Specimens I.1 and II.1 satisfied the AISC push protocol [2] and the minimum required cumulative ductility of 200, with values of 1804 and 369, respectively (Table 3.1). Specimens I.2 and II.2 passed the European push protocol [5] several times, 6 and 5 respectively.

Fig.3.11 shows the plastic cumulative ductility versus the ductility of the yielding core. Based on MBRB results [41] a correlation between both parameters was expected, but this was not to be the case. Experimental results show that failure is mostly related to maximum deformation and ductility. Ductility values from 14 to 18 are obtained when all the specimens are considered. The ductility range narrows to 16-18 for the specimens that satisfy the design equation (Eq.3.5). For design purposes a maximum ductility of 8 [2] should be considered.

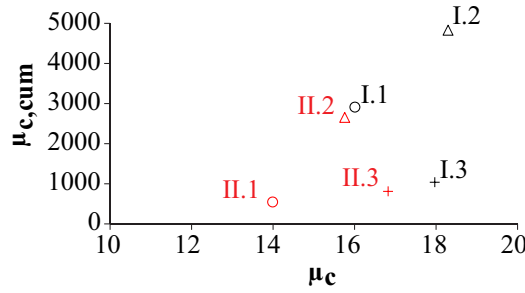


Figure 3.11: Cumulated ductility($\mu_{c,cum}$) vs ductility(μ_c)

Table 3.1 summarizes the experimental results of the specimens. $\delta_{c,y}$ and $\delta_{b,y}$ are the yielding displacements of the core and the brace, respectively. T_{max} and C_{max} are the maximum tension and compression forces, respectively. $\delta_{c,max}$ is the maximum deformation of the core, δ_{cum} is the cumulated plastic deformation, μ_c is the ductility of the core ($\frac{\delta_{max}}{\delta_{c,y}}$). $\mu_{c,cum}$ is the cumulative ductility of the core ($\frac{\delta_{cum}}{\delta_{c,y}}$), and $\delta_{b,cum}$ is the cumulative ductility of the brace ($\frac{\delta_{cum}}{\delta_{b,y}}$). E_t is the hysteretic energy. The cumulative displacement δ_{cum} is obtained as $\sum 2(\delta_{c,i}^+ + \delta_{c,i}^-) - 4\delta_{c,y}$ [36].

	I.1	I.2	I.3	II.1	II.2	II.3
F_y (kN)	117	109	108	106	116	111
$\delta_{c,y}$ (mm)	0.96	1.02	0.98	1.00	1.20	1.05
$\delta_{b,y}$ (mm)	1.55	1.90	1.40	1.48	1.49	1.30
T_{max} (kN)	168	164	177	169	168	174
C_{max} (kN)	-197	-209	-236	-190	-200	-191
F_{max}/F_y	1.68	1.92	2.57	1.79	1.72	1.73
β	1.17	1.27	1.33	1.12	1.19	1.10
$\delta_{c,max}$ (mm)	15.69	17.93	17.61	15.11	17.02	18.17
δ_{cum} (mm)	2797	4378	1040	546	2657	812
μ_c	16.01	18.30	17.97	14.00	15.76	16.82
$\mu_{c,cum}$	2914	4831	1040	546	2657	812
$\mu_{b,cum}$	1804	2304	743	369	1783	625
E_t (kJ)	312	407	127	62	339	98

Table 3.1: Summary of the experimental results of the specimens

The experimental behaviour of specimen I.3 has been compared with two conventional BRBs tested by Newell et al. [36] under the same protocol in terms of normalized hysteretic energy ($E_t^* = \frac{E_t}{F_y \delta_{b,y}}$), cumulative ductility and β . Similar values were found (Table 3.2).

	E_t^*	$\mu_{b,cum}$	β
SSBRB I.1	1720	1804	1.17
BRB 1 [36]	1597	1143	1.17
BRB 2 [36]	1480	1083	1.28

Table 3.2: Comparison between an SBRB and conventional BRBs [36]. Normalized hysteretic energy (E_t^*), cumulative deformation ($\mu_{b,cum}$) and coefficient β

3.5 Numerical analysis

The main objectives of the numerical model is to study the behaviour of the brace during the first cycles and examine the interaction between the core and the restraining unit. Commercial finite element software ABAQUS/Explicit 6.12 [7] is used.

The model consists of the core, the slotted part of the restraining unit and the exterior pin connection (Fig. 3.12). All parts are modelled using C3D8R

elements. The same push protocols used on the specimens are also used to load the numerical models.

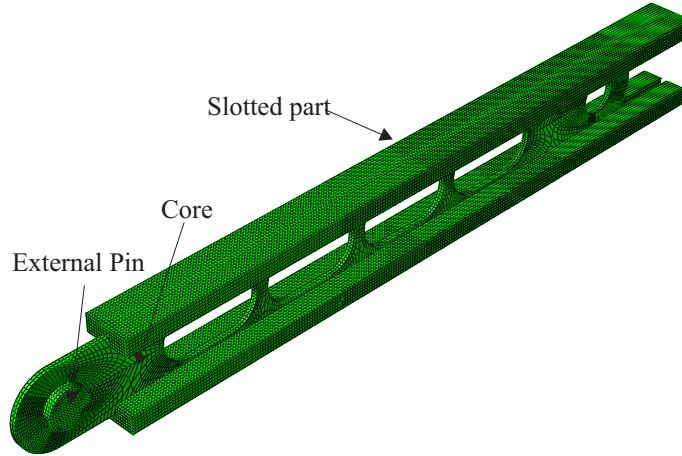


Figure 3.12: Numerical model parts and mesh

The material is defined using the ABAQUS kinematic and isotropic combined model. Data used to create the model is obtained by tension tests according to [3] and it is shown in Table 3.3.

Stress [MPa]	267	397	476	548	555
Strain [mm]	0	0.03	0.08	0.17	0.21

Table 3.3: Material data used on numerical model

Contour conditions on the slotted part are applied by clamping its exterior nodes. To simulate the interior pin connection, a virtual node in the center of the hole is created. The nodes of the hole are then coupled to this node and rotate on its axis (Fig. 3.13). The exterior connection is modelled using a pin and with this the interaction between this element and the core can be considered. Simulation is done with displacement control. Displacement δ_c is applied to the pin of the external connection.



Figure 3.13: Contour conditions of the core

The general contact rule is used to model the contacts between the elements. Friction is added using an exponential law, which provides smooth transition between the static and dynamic friction coefficients, their values being 0.2 and 0.1, respectively.

The model is able to reproduce the first cycles of the test (Fig. 3.14). It is particularly effective in determining the displacement and the yielding force (Fig. 3.15). Table 3.4 shows a comparison between the numerical, analytical and experimental results of the core at yielding point. The numerical model's chief shortcoming is that it is not able to accurately reproduce the hardening under a large number of cycles.

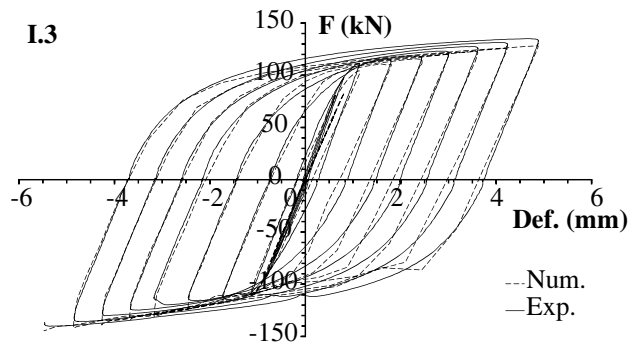


Figure 3.14: Comparison between the hysteretic behaviour of the numerical model and specimen I.3 during the first cycles

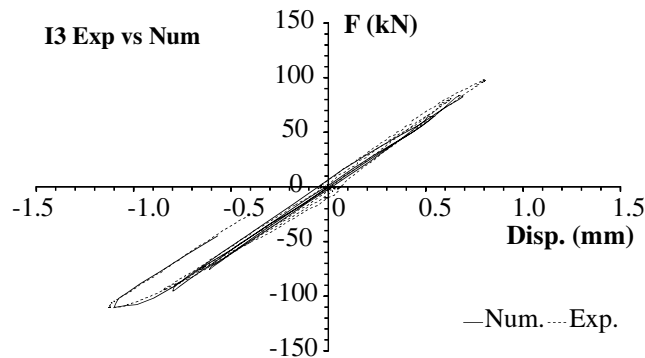


Figure 3.15: Numerical vs experimental behaviour at the yielding point of specimen I.3

Fig. 3.16 shows Von Mises stress distribution of specimen I.3 with the brace in tension. Here the stabilizing zones remain on the elastic range, while the lateral

¹Experimental mean value

	F_y (N)	Δ_y (mm)
Eq. (3.1) (3.3)	107	0.86
Exp. ¹	111	0.98
Num.	110	0.87

Table 3.4: Comparison between the analytical, experimental and numerical values at the yielding point

bands exceed the yielding stress.

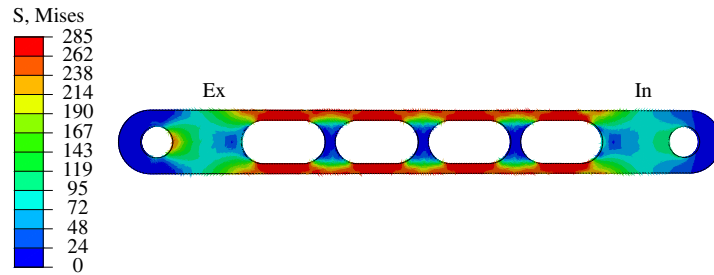


Figure 3.16: Core stress distribution of specimen I.3 at peak tension force on the third test cycle

The evolution of the strain distribution along the lateral bands at peak tension displacements in successive cycles is shown in Fig. 3.17. As can be seen in the first cycles, the strain is near uniformly distributed. After several cycles the external zone has smaller strains than the internal one. A model without friction did not show this effect, so the non-uniform distribution of the strains is caused by the friction between the core and the restraining unit. Non-uniformity on strain distribution justifies the experimental failure of specimens, with larger second order effects and buckling in the external zone of the lateral band and tensile failure in the internal zone. It can be stated that friction has to be considered for a proper modelling of the hysteretic behaviour.

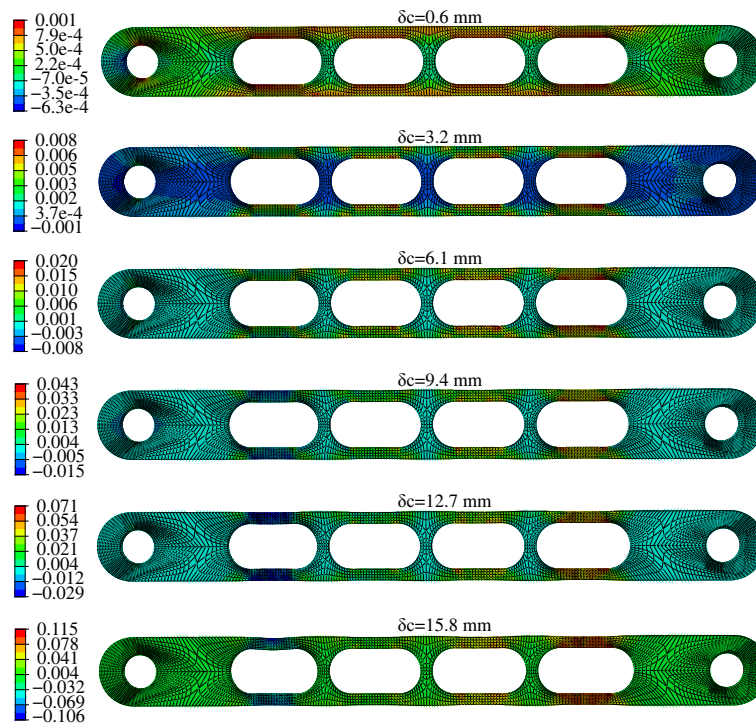


Figure 3.17: Evolution of the axial strains from the FEM analysis of specimen I.3

Fig. 3.18 compares the deformation of Type I and Type II specimens after several cycles. Type II exhibits a higher deflection in the external zone than Type I. Deformations in the numerical model are coherent with those obtained experimentally (Fig. 3.10).

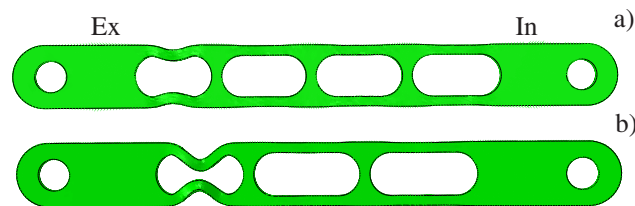


Figure 3.18: Deformation under tension force of numerical model of specimens I.3 and II.3 after several cycles

In Fig. 3.19, both the in-plane deformation and out-of-plane deformation of specimen I.3 are shown. Out-of-plane deformation causes the interaction between the core and the encasing member and the friction forces, whereas the in-plane deformation is responsible for the loss of compression capacity in specimens II.1

and II.3. The evolution of maximum in-plane displacement (δ_{IP}) versus the axial deformation of the core (δ_c) is detailed in Fig.3.20. The in-plane displacement increases when a large axial deformation of the core is achieved, although this effect is less important in specimen Type I than in Type II.

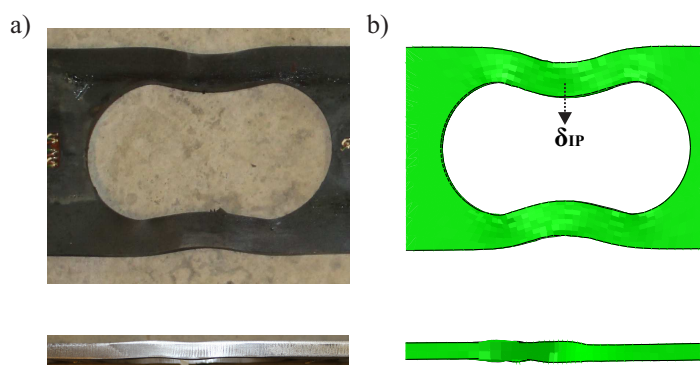


Figure 3.19: Out-plane and in-plane (δ_{IP}) displacement of the numerical model of specimen I.3 after several cycles

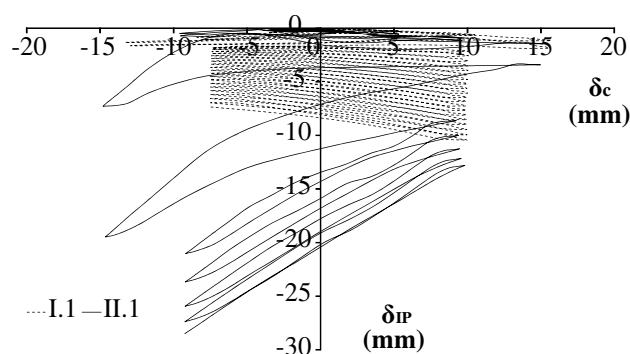


Figure 3.20: In-plane displacement vs the core deformation for FEM models of the specimens I.1 and II.1

3.6 Summary and conclusions

The new Slotted Buckling Restrained Braces (SBRB) which have as yielding cores two steel plates guided and partially stabilized by internal slots in the restraining unit, were designed and tested both numerically and experimentally. The cores and the restraining casing are connected by internal pins to transmit the axial forces from both of the external brace connections. Instead of having a solid slender bar as a yielding core, as conventional BRBs have, the SBRB's core is

a partially emptied plate which is shaped to allow the two lateral bands to be connected by equidistant transverse stabilizing bridges. The lateral bands are designed to yield to axial forces, as conventional BRBs do, while the stabilizing bridges are designed to remain elastic and, along with the slots in the restraining unit, hold the lateral bands stable under compression.

The force and displacement at the yielding point can be obtained from the assumption of uniform axial stress in the lateral bands. To distribute stabilizing zones along the lateral band an expression based on Euler's formulation is proposed. Based on the proposed formulation, two types of specimens (Type I and Type II) have been designed and tested. Those with a greater distance between the stabilizing bridges (Type II) are more susceptible to local buckling and thus a lower ductility. The ductility range obtained from all tested specimens ranges from 14 to 18, and narrows to 16 to 18 when the stabilizing bridges are properly distributed.

Six specimens with protocols defined by AISC341-05 [2], EN15129 [5] and a loading protocol consisting of cyclic deformation with increasing amplitude were all tested to failure. All of the Type I specimens exhibited a stable response, while two of the Type II specimens showed a progressive loss of the compression capacity produced by local buckling and they dissipated less energy. The response of the SBRB has been compared to two conventional BRBs, in terms of the normalized hysteretic energy and cumulative ductility, and similar values have been found.

Finally, a numerical model to study the interaction between the core and the encasing member has been defined. The model is able to accurately reproduce the hysteretic response during the first cycles, and its deformation is coherent with the experimentally obtained results. It shows that during the first cycles the strain is uniformly distributed along the lateral bands. However, after several cycles friction forces propel a non-uniform distribution of the strain that is coherent with the experimental failure of specimens, with buckling in the exterior zone of the lateral bands when stabilizing bridges are too distant, and with tensile failure in the interior zone in the opposite case. However, as the material model is not well developed for a high number of cycles, it is unable to reproduce the experimental hardening of steel.

3.7 Acknowledgements

This work has been supported by the Spanish Government under Project MEC BIA2011 26816. The research group of AMADE (University of Girona) and Bellapart Company (Olot - Spain) have collaborated in the manufacturing and testing of the specimens. Their help is gratefully acknowledged.

Chapter 4

A constitutive model for simulating all-steel buckling restrained braces

This chapter contains the transcription of the submitted paper:

Daniel Piedrafita; Pere Maimí, Xavier Cahis. *A constitutive model for simulating all-steel buckling restrained braces* Submitted to Engineering Structures.

Impact index 1,713. Journal 18 of 122, 1st quartile, Category: Engineering, Civil

Abstact

Buckling Restrained Braces (BRB) have been demonstrated as being very effective for building protection in seismic events. The modelling of all-steel BRBs is presented here in this work. The hysteretic behaviour is simulated using a combined isotropic and kinematic hardening, with the particularity that the relationship between them evolves as long with the amount of plastic flow. The damage is introduced using an uncoupled analysis, the evolution of this is formulated using an existing model based on a continuum damage mechanism model. To adjust and verify the model, results from tensile steel and all-steel BRB tests are used. Both the load-deformation response and failure prediction of the proposed models have been well correlated with the experimental results.

4.1 Introduction

Buckling restrained braces (BRB) are a solution used to improve buildings the response in seismic actions [45]. Like conventional restraining braces these devices are installed inside the structure. However, they not only limit the lateral displacement of the structure, but they also dissipate the energy coming from the seismic action. In conventional BRBs a slender steel core yields to dissipate energy, and this core has to be restrained to avoid buckling under the compression forces. Fig. 4.1. Conventional BRB are composed of a steel core encased by a restraining unit manufactured with a standard a standard mortar-filled profile [52].

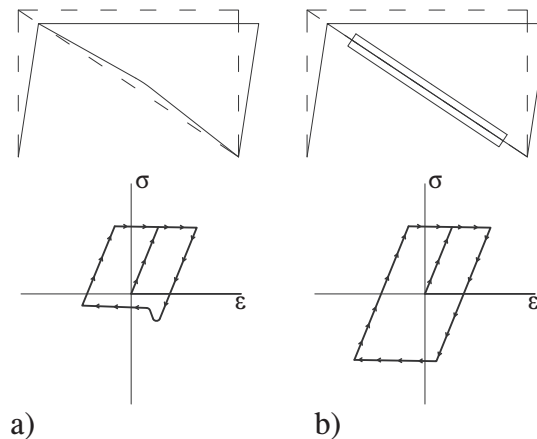


Figure 4.1: Comparison between the behaviour of the restraining brace without a) and with b) the encasing member

The way to prove its effectiveness is with experimental tests, but they are expensive and involve a great deal of work. To have accurate modelling tools using data from simple tests, as with the tensile test, would result in a drastic reduction in testing costs. Developing such tools is a challenging objective for researchers and brace designers. To model the behaviour of a BRB means not only to predict the force-deformation hysteretic response, but also its dissipation capacity before failure. And this must be done taking into account large plastic deformations on the steel, second order effects, and also considering mortar cracking and the steel-rubber-concrete interaction between the core and the encasing member of the brace in conventional mortar-filled BRBs, consequently conventional BRBs difficult to simulate. Several models have been developed to specifically simulate conventional BRB behaviour. One example is the numerical model presented by

López-Almansa et al. [33], which includes metal plasticity, either using isotropic or kinematic hardening, with isotropic damage, governed by a scalar damage index, for the steel core and the same isotropic damage model for the mortar of the encasing member. A further option for reproducing the behaviour of the conventional BRBs would be the macroscopic model, proposed by Zona and Dall'Asta [57] based on a rheological scheme.

All steel BRBs are easier to simulate than conventional BRBs as the interaction between the encasing member and the core do not involve mortar cracking and the traditional rubber or silicone layer is substituted by an air gap. Several models of metals behaviour under large strain cyclic plasticity have been developed. Yoshida [53] describes a viscoplastic constitutive model to simulate the behaviour of steel under large plastic deformations. Following on from this, the author improves the model by defining a two surface model [54] and verifies it using steel sheets under cyclic deformations [55]. Kim et al. [28] also propose a two surface model, but this is specifically developed for reproducing the behaviour of metallic plate dampers and includes a damage parameter (dependent on the dissipated energy) which they suggest it can be used as an index for the damaged state of material. Martinez et al. [35] propose a plastic damage model based on the combination of isotropic and kinematic hardening and also introduce a damage variable which is able to predict the material failure. Bonora [15] defines a model with isotropic hardening and based on Continuum Damage Mechanisms (CDM) to reproduce ductile failure. Bonora and Newaz [14] add kinematic hardening to the model and extend this to low cycle fatigue, proposing that damage only increases under tension deformations. They also study the effects on the response of coupled damage. Bonora et al. [16] validate the model (only with isotropic hardening) for using it in structures under a multi-axial state of stress. Finally, Pirondi et al. [42] ran several tests and simulations to compare this model (with combined isotropic-kinematic hardening) with the other CDM model [30].

The models available for ductile materials on the commercial finite element software ABAQUS [7] are easy to use, but they are not able to properly simulate the behaviour of the BRB. The isotropic model Fig. 4.2 a) is not able to approximate the real behaviour so as not reproduce the Bauschinger effect [34]. The kinematic model implemented in this software is linear, so its ability to reproduce real behaviour is limited. The combined isotropic and kinematic hardening model Fig. 4.2 b) is not defined to reproduce material behaviour after several

cycles of long plastic deformation [7]. Despite this, the combined model is useful for simulating monotonic loads [21] or during the first cycles [41] of a cyclic test.

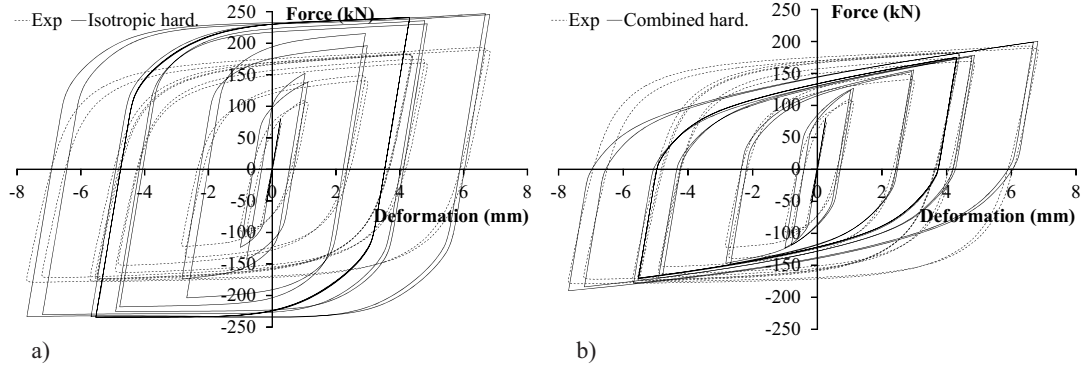


Figure 4.2: a) ABAQUS [7] isotropic hardening model and b) ABAQUS [7] combined hardening model applied to MBRB [41]

This paper proposes a material model able to approach the behaviour of an all-steel BRB. The formulation, the implementation and an example of usage based on the all-steel BRB developed by Piedrafita et al. [41] is presented. This model is defined using an implicit integration algorithm with a combined kinematic and isotropic hardening, the portion of each is related to the amount of plastic flow. The damage is introduced into the model using an uncoupled analysis in the form of a failure criteria based on the continuum damage mechanisms model as defined by Bonora and Newaz [14]. The calibration of the hardening parameters is done using the results from material tensile tests, while the evolution of the relationship between the kinematic and isotropic hardening is adjusted empirically. The damage model is adjusted using available bibliography data [42]. The material model is verified using experimental data from the tensile steel test in order to study the response under monotonic load, and from the all-steel buckling restrained brace tests [41] so as to obtain the hysteretic response.

4.2 Constitutive model

4.2.1 Plasticity

The additive decomposition of the strain tensor ε_{ij} is:

$$\varepsilon_{ij} = \varepsilon_{ij}^E + \varepsilon_{ij}^P \quad (4.1)$$

where ε_{ij}^P and ε_{ij}^E are the plastic and elastic strain tensors, respectively.

Within Von Misses concept, a yield criterion of mixed hardening is considered [38]:

$$f(s_{ij}, \alpha_{ij}, K) = \sqrt{\frac{3}{2}} \|s_{ij} - \alpha_{ij}\| - \sigma_y - K(r) \leq 0 \quad (4.2)$$

where σ_y is the yielding stress, r an internal hardening variable, s_{ij} is the stress deviator, α_{ij} is the kinematic hardening tensor and $K(r)$ is the function that defines the evolution of the isotropic hardening. Fig. 4.3 shows the evolution of the yielding surface in the stress space.

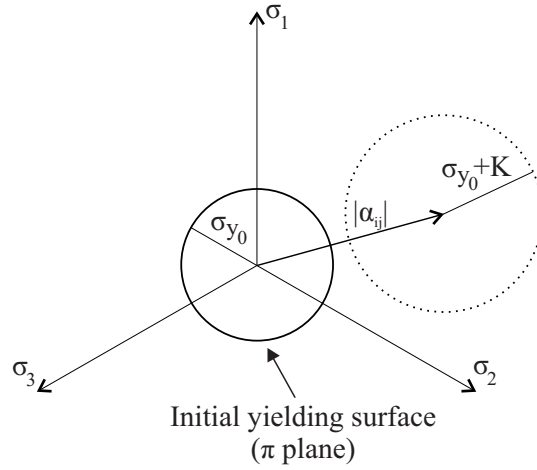


Figure 4.3: Evolution of the yielding surface

The evolution of the internal variables can be described using the scalar r by the flow rule, Eq. 4.3.

$$\dot{\varepsilon}_{ij}^P = \dot{r} \frac{s_{ij} - \alpha_{ij}}{\|s_{ij} - \alpha_{ij}\|} \quad (4.3)$$

where $\alpha_{ij} = \beta \varepsilon_{ij}^P$ and β is a function which defines the kinematic hardening.

4.2.2 Damage

The damage is introduced into the model using the formulation defined by Bonora and Newaz [14] and an uncoupled analysis as proposed by the same authors. This formulation is based on the continuum damage mechanisms model. Hence, the damage variable takes into account the effects of the irreversible processes in the micro-structure of the material (evolution and creation of the voids), as well as in

the damage on the macro scale (macro crack). The authors define the behaviour of the damage variable (D) as:

$$\dot{D} = \alpha' \frac{(D'_{cr} - D_0)^{(1/\alpha')}}{\ln(\varepsilon_{cr}/\varepsilon_{th})} \left(\frac{2}{3}(1 + \nu) + 3(1 - 2\nu) \left(\frac{\sigma_H}{\sigma_{eq}} \right)^2 \right) (D_{cr} - D)^{\frac{(\alpha'-1)}{\alpha'}} \dot{\gamma} \quad (4.4)$$

where D'_{cr} is defined as 1 [14] and D_0 is the initial damage, ε_{th} is the strain at which damage starts, ε_{cr} is the failure strain from the tensile test, ν is the poisson coefficient, α' is a material parameter which defines the shape of the damage curve, σ_H and σ_{eq} are the hydrostatic stress and the Von Mises stress, respectively. Critical damage (D_{cr}) is the value of D where the evolution of the voids in the micro-structure drives the appearance of the macro crack and consequently the failure of the material. Lemaitre and Desmorat [31] propose to obtain this by using the tensile test data as:

$$D_{cr} = 1 - \frac{\sigma_R}{\sigma_u} \quad (4.5)$$

where σ_R and σ_u are the rupture and the maximum stress obtained in tensile tests, respectively.

4.3 Implementation

4.3.1 Algorithm

Algorithm entries are the current step deformation ε_{n+1} and the set of the internal variables (\bullet) from previous step: ε_n^P , ε_n^E , α_n and r_n . The outputs of the algorithm will be the updated values of the internal variables, stress tensor and the constitutive tangent tensor. The algorithm works following the subsequent steps:

1. Compute elastic trial state
2. IF $f_{n+1} \leq 0$ THEN
Elastic step: $(\bullet)_{n+1} = (\bullet)_n$ & EXIT
3. IF $f_{n+1} > 0$ THEN
Plastic step: GO TO Step 4

4. Return mapping algorithm
 WHILE ABS(f_{n+1}) < TOLER DO
 Increment of plastic parameter:

$$\Delta r = \frac{f_{n+1}}{\frac{3}{2}(2G+\beta)}$$
 Update the internal variables

$$r_{n+1} = r_n + \Delta r$$

$$\Delta \varepsilon_{ij}^p = \frac{s_{ij} - \alpha_{ij}}{\|s_{ij} - \alpha_{ij}\|} \Delta r$$

$$(\varepsilon_{ij}^p)_{n+1} = (\varepsilon_{ij}^p)_{n+1} + \Delta \varepsilon_{ij}^p$$

$$(\varepsilon_{ij}^E)_{n+1} = (\varepsilon_{ij}^E)_{n+1} - \Delta \varepsilon_{ij}^p$$

$$\dots$$

$$(\alpha_{ij})_{n+1} = (\alpha_{ij})_{n+1} + \beta \Delta \varepsilon_{ij}^p$$

$$f_{n+1}$$

where "TOLER" is the loop break value (10^{-6}) and G is the shear modulus.

4.3.2 Tangent operator

The tangent operator is defined as the relationship between the increment of stresses $\dot{\sigma}$ in the face of the increment of the strains $\dot{\varepsilon}$ (Eq. 4.6). This operator provides a good convergence, which is necessary when the model is implemented in a finite element method code.

$$\dot{\sigma}_{ij} = C_{ijkl}^T \dot{\varepsilon}_{kl} \quad (4.6)$$

From the flow rule (Eq. 4.3) and the yielding function (Eq. 4.2), the tangent operator is obtained:

$$C_{ijkl}^T = C_{ijkl} - \frac{9G^2}{3G + \frac{3}{2}\beta + \frac{3}{2}\frac{\partial K}{\partial r}} \frac{s_{ij} - \alpha_{ij}}{\|s_{ij} - \alpha_{ij}\|} \frac{s_{kl} - \alpha_{kl}}{\|s_{kl} - \alpha_{kl}\|} \quad (4.7)$$

4.4 Model adjustment

The model response is determined by the definition of the functions $K(r)$ and $\beta(r)$ which define the isotropic and the kinematic hardening laws, respectively.

This response can be expressed using the following equations:

$$\bar{\sigma} = K + B + \sigma_y \quad (4.8)$$

$$m = \frac{K}{K + B} \quad (4.9)$$

where $\bar{\sigma}$ represents the hardening law, and m is the relationship between the isotropic and the kinematic hardening. So if $m = 1$ the model is purely isotropic hardening, and if $m = 0$ it is purely kinematic hardening and B is a hardening function defined as $B = \sqrt{3/2} \int \beta(r) dr$.

Considering that the hardening law is expressed by:

$$\bar{\sigma} = \sigma_y + \xi_F (1 - e^{-\xi_E r}) + \xi_L r \quad (4.10)$$

and the relation between the isotropic and the kinematic hardening is defined according:

$$m = m_F + (m_0 - m_F) e^{-m_P r} \quad (4.11)$$

then β is:

$$\beta = \sqrt{\frac{2}{3}} ((\bar{\sigma} - \sigma_y) (m - m_F) m_P + (1 - m) (\xi_F \xi_E e^{-\xi_E r} + \xi_L)) \quad (4.12)$$

where m_i and x_{i_i} are material constant values.

Under uniaxial loading, the internal hardening variable (r) is related with the plastic deformation ε_{11}^P according to:

$$\varepsilon_{11}^P = r \sqrt{\frac{2}{3}} \quad (4.13)$$

The response of the model is adjusted using the results from a S275JR [1] steel tensile test. To simulate the tensile test, a rectangular part meshed with C3D8 solid elements is used. Fitting the hardening law $\bar{\sigma}$ (Eq. 4.10) is obtained using the MATLAB fitting tool [8]. Parameters of function m (Eq. 4.11) are adjusted empirically using all-steel MBRB experimental data [41]. Table 4.1 shows the constant values of the material. The failure criteria is adjusted according to the values provided by Pirondi et al. [42] for a similar material, and these values are shown in Table 4.2.

E	ν	σ_y	σ_u	ξ_F	ξ_E	ξ_L	m_0	m_F	m_P
205000	0.3	279	420	192.3	24.59	454.3	0.3	0.07	0.6

Table 4.1: Constant values of the material

α'	D'_{cr}	D_0	ε_{cr}	ε_{th}	D_{cr} (Eq.4.5)
0.22	1	0	1.5	0.0213	0.21

Table 4.2: Constant values of damage model [42]

Fig. 4.4 shows the response of the modelled material compared with the experimental data under the tensile test. The evolution of the damage variable D in the element located in the center of the necking is also represented.

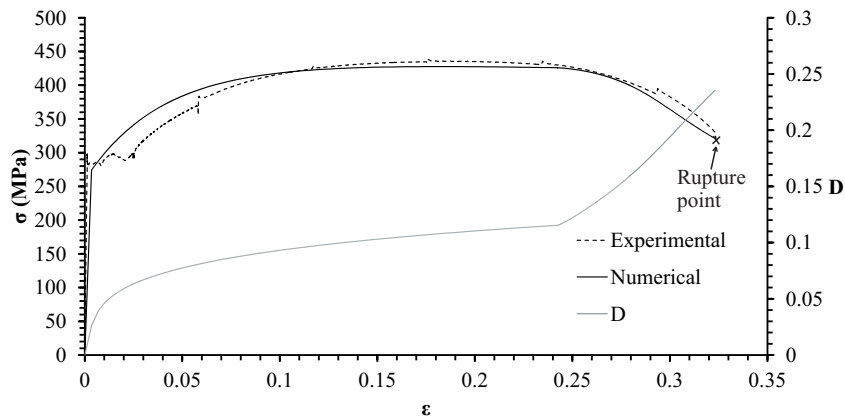


Figure 4.4: Response of the modelled material vs. an experimental result from the tensile test. The evolution of damage variable (D) in the central element of the necking is in grey

How the numerical model is able to reproduce the overall behaviour of the test can be observed. The damage value provided by the model at the failure displacement ($D = 0.24$) of the experimental specimen is close to D_{cr} provided by Eq.4.5. As bibliographical data is used to calibrate it, then specific tests can improve the result.

4.5 Modelling of an all-steel BRB

The model proposed earlier on, is applied in order to predict the load-deformation hysteretic curve and the damage of an all-steel BRB, which had been previously

tested by Piedrafita et al. [41], and numerical and experimental results are then compared. The concept, design and experimental behaviour of this brace is reported in [41]. Fig. 4.5 a) shows the core of the brace, which is the dissipative part. This is guided by the external restraining unit and it is composed of several seriated connected units (SM). They are identified as SM1, SM2 and SM3. Fig. 4.5 b) shows one of the seriated connected units and indicates the geometry and parameters of the unit. The values of the main parameters of the core are $d = 55$ mm, $h = 87.5$ mm, $b_w = 39$ mm, $b_f = 28$ mm, $t_f = 8$ mm, $t_{wSP1} = 2.64$ mm, $t_{wSP2} = 2.50$ mm and $t_{wSP3} = 2.67$ mm. The differences in the values of t_w between the specimens are caused by manufacturing imperfections [41]. The core of the material is the same as was used in the tensile tests (Tables 4.1 and 4.2).

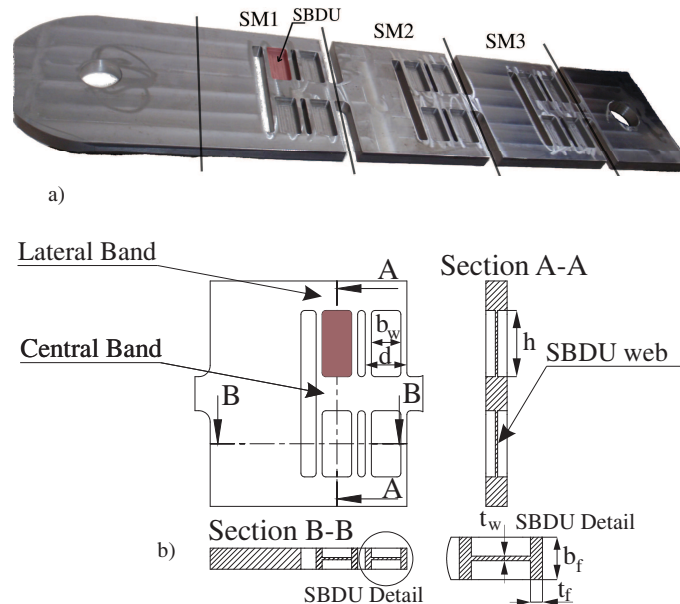


Figure 4.5: (a) Modular Buckling Restrained Brace core geometry (b) Seriated Module (SM) detail [41]

The specimens were submitted to three push protocols as depicted Fig. 4.6: AISC341-05 [2] (Specimen 1), EN15129 [5] (Specimen 2) and a cyclic deformation with increasing amplitude (Specimen 3). Position traducers measured the displacement of each SM.

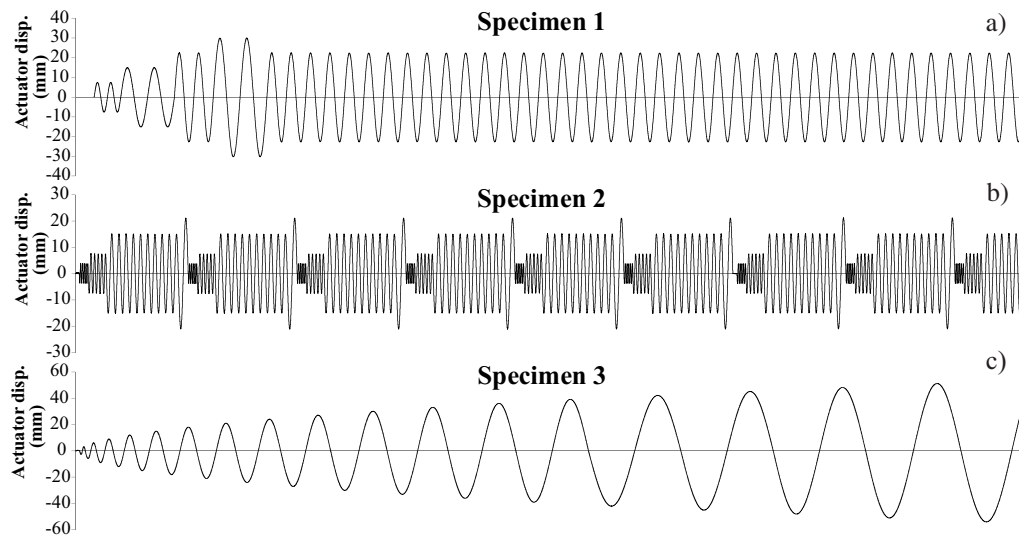


Figure 4.6: (a) AISC341-05 [2] protocol (b) EN15129 [5] (c) cyclic deformation with increasing amplitude [41]

The numerical model includes the SM which failed in each experimental test and the geometry is modelled using C3D8 solid elements (see Fig. 4.7). As is shown in the figure, the boundary conditions are applied at the two ends of the SM. On one side the nodes are clamped to simulate the connection with the next SM and on the other only horizontal movement is allowed so as to apply the same displacement obtained from the data of the position transducers used in the experimental specimens [41]. The model includes the geometrical imperfections from the machining process in the form of different thickness of each SBDU. The material data is the same as shown in Table 4.1. The experimental response is compared with the response of the numerical model for each specimen (Fig. 4.8).

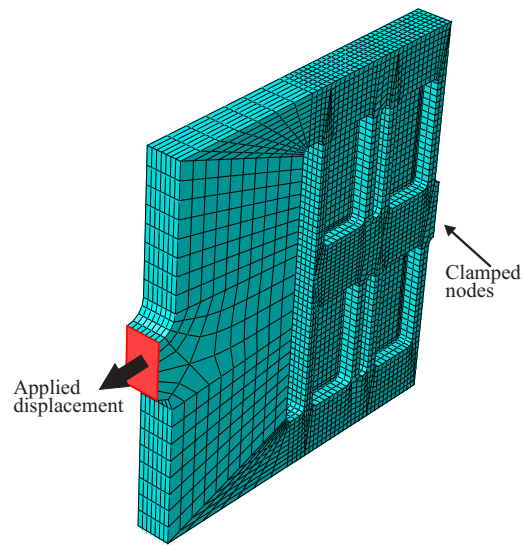


Figure 4.7: Mesh and boundary conditions of the numerical model

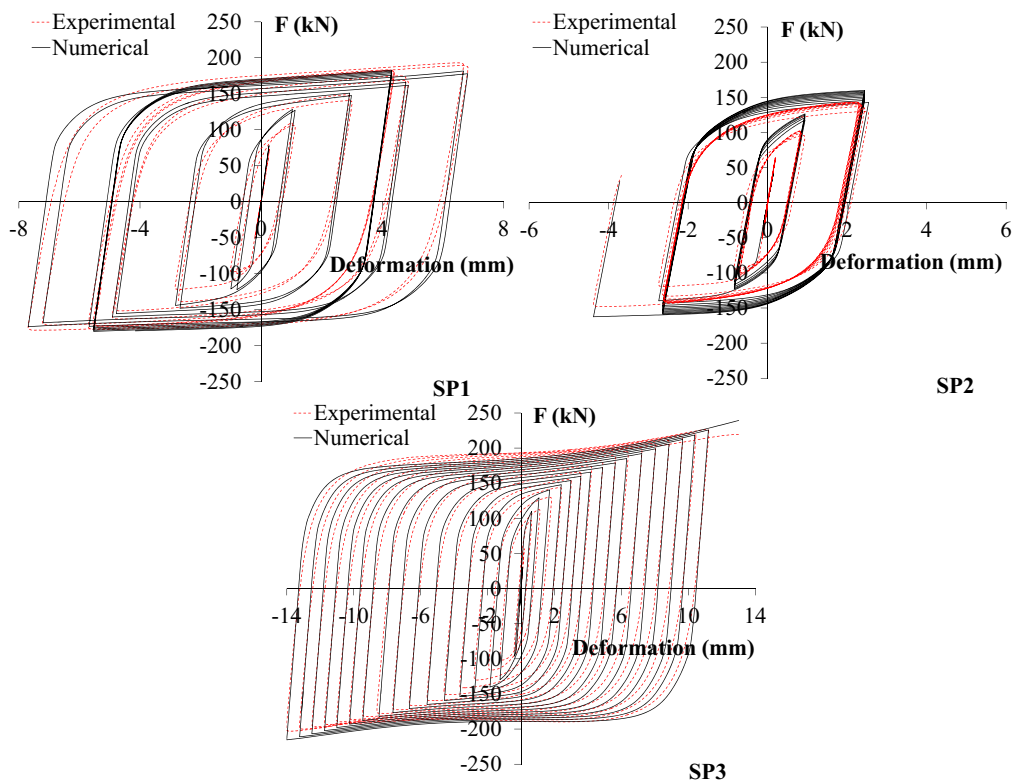


Figure 4.8: Comparison between experimental and numerical behaviour of the three specimens

The numerical model is able to simulate the global behaviour of the BRB core in all three cases. To validate the damage model, the numerical model of each specimen has been submitted to the same protocol displacement that drove the failure of the experimental specimens. Fig. 4.9 a) is a photo of the failure of the shear dissipation zone of the seriated connected unit for one of the tested specimens, Fig. 4.9 b) shows the amount of plastic flow (r) distribution and Fig. 4.9 c) shows the damage variable (D) values of the numerical model at maximum traction displacement. How the zone with maximum values of D in the numerical model agree with the experimental specimen failure mode can be observed. Fig. 4.10 contains a graphic with the evolution of the damage variable (D) versus the core deformation (u) during the virtual test of each specimen in the element that reaches the maximum value of D . In all of the cases the damage variable provides a value near to that defined by D_{cr} when the failure point of the applied protocol in experimental specimens is reached.

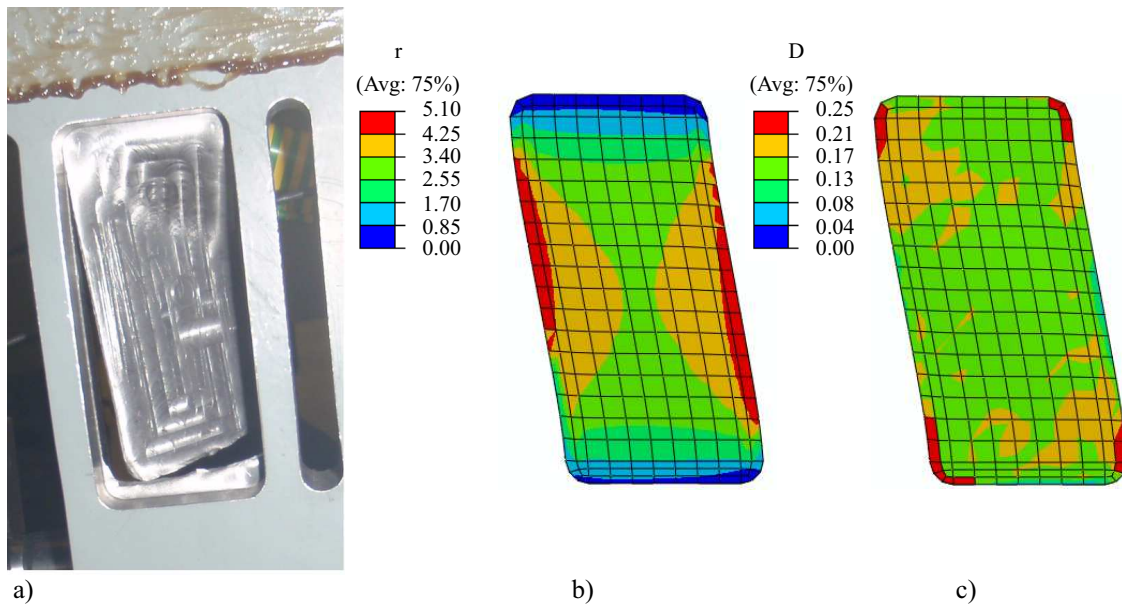


Figure 4.9: a) Photo after failure of tested specimen b) Amount of plastic flow (r) and c) Damage variable (D) distribution at maximum displacement on traction of numerical model of specimen 3

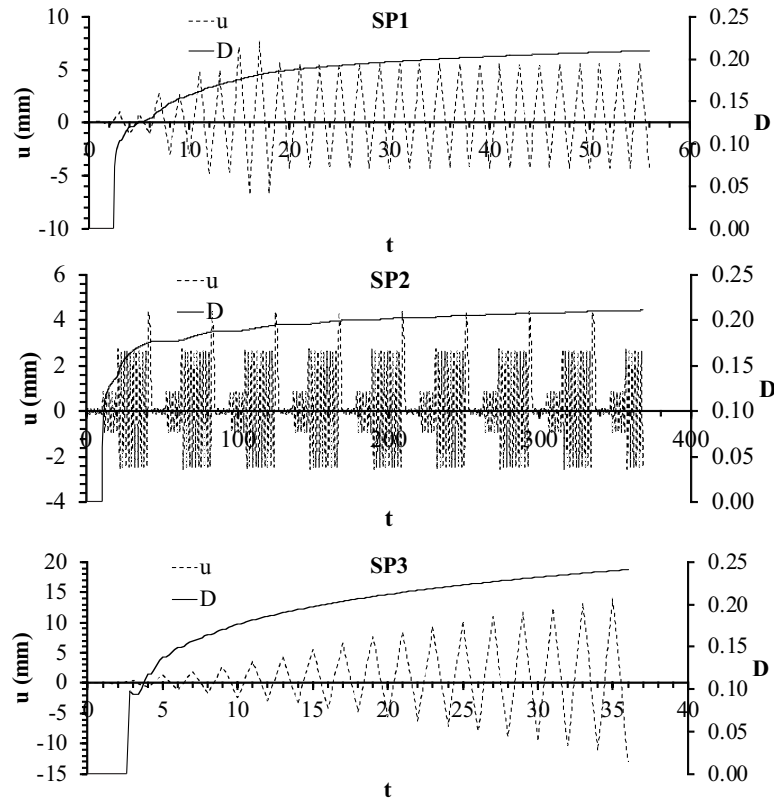


Figure 4.10: Damage variable (D) evolution compared with core deformation (u)

4.6 Summary and conclusions

In this paper a material model to simulate the hysteretic behaviour of an all-steel BRB submitted to low cycle fatigue is proposed. This model has two steps; in the first one the hysteretic behaviour is modelled using a hardening rule based on a combination of isotropic and kinematic hardening, with the particularity that the relationship between these evolves along with the amount of plastic flow. The hardening law is adjusted using the traction test data and the evolution of the portion of the two types of hardening is adjusted using the experimental data from the all-steel BRB tests. In the second step the damage is incorporated as a post-process variable. The evolution of this variable is modelled using a continuum damage model formulated by Bonora and Newaz [14] and adjusted using available bibliographical data.

The material model is implemented in the commercial finite element software ABAQUS [7] to be later used in implicit analysis. It is adjusted and verified using a steel tensile test and all steel BRB tests [41]. The model is able to re-

produce the response of the material under a tensile test. As to the hysteretic behaviour of the all-steel BRB, the model reproduces the overall response. In the case of the damage model, while it provides an approximation of the failure point reached during the experimental tests in both cases, even when using available bibliographical data. Specific material characterization tests for model damage parameters identification could improve the results of the failure point identification.

4.7 Acknowledgements

This work has been supported by the Spanish Government under Projects MEC BIA2011 26816 and MAT2013-46749. The research group AMADE (University of Girona) and the Bellapart Company (Olot - Spain) have collaborated with the research work and their help is gratefully acknowledged.

Chapter 5

Discussion and conclusions

The use of Buckling Restrained Braces (BRBs) is a wide-spread solution used to improve the response of buildings under seismic actions. These devices dissipate the earthquake energy input by means of the yielding of their metallic cores. Conventional BRBs use mortar to achieve dimensional compatibility between the restraining unit, which avoids the buckling of the yielding core under compression forces, and the yielding core. The use of mortar results in heavy weight elements, a complex manufacturing process and, after being damaged the core cannot be inspected and substituted if necessary.

In this present work, initially two innovative non-conventional BRBs are designed, tested and modelled. Their main characteristics are that they are all-steel BRBs, their restraining units are manufactured with several steel bars which are welded to form a hollow element providing a guiding element to the core thus avoiding the use of mortar. The debonding material is replaced by an air gap and a greased layer between the steel faces. The main conclusions of each brace are exposed next:

In Chapter 2, a Modular Buckling Restrained Brace (MBRB) is designed and tested. The yielding cores are modular and consist of several Shear Basic Dissipation Units (SBDUs) grouped into several Seriated Modules (SMs). The axial force of the MBRB is proportional to the number of SBDUs at each SM and to SBDU force. The deformation of the MBRB is proportional to the number of SMs and to the deformation of the SBDUs. Several expressions have been proposed to predict the force and the deformation at the yielding and ultimate points. These expressions have been adjusted and validated using the experimental results. Three specimens have been tested under different test protocols until their failure is reached. The hysteretic curve of the tested specimens is stable and symmetrical. However, as the plastic deformation is not uniformly extended, and contrary to conventional BRB, the MBRB has to be heavier than a conventional BRB to obtain the same energy dissipation capacities.

To solve the main shortcoming of the MBRB; the heavier weight when it is compared with the conventional BRBs, in Chapter 3 a Slotted Buckling Restrained Brace (SBRB) is designed and tested both numerically and experimentally. The SBRBs core is a partially emptied plate which is shaped to allow the two lateral bands to be connected by equidistant transverse stabilizing bridges. The lateral bands are designed to yield to axial forces, as conventional BRBs do, while the stabilizing bridges are designed to remain elastic and, along with

the slots in the restraining unit, hold the lateral bands stable under compression. Expressions to size the SBRB core are proposed and verified testing two families of cores. Tests have done under different loading protocols until failure is reached to characterize their behaviour experimentally. A numerical model to study the interaction between the core and the encasing member has been defined. The model is able to accurately reproduce the hysteretic response during the first cycles, and its deformation is coherent with the experimentally obtained results.

Finally, a constitutive model for simulating the behaviour of the all-steel buckling restrained braces developed in chapter 2 is formulated and implemented in a commercial finite element method software and verified using experimental data. The plastic region is simulated with a combination of isotropic and kinematic hardening, the portion of each one evolving with the amount of plastic flow. Damage is introduced as an uncoupled analysis using a continuum damage mechanism model. The material model is adjusted and verified using the experimental data from the material tensile and all-steel BRB tests. It is able to reproduce the overall behaviour of experimental specimens in both cases and provides a good approximation to the failure point reached during the experimental tests.

As a result of the research work represented here, the following future work is suggested:

- Improving the SBRB design to avoid the initial flexure in the outer lateral bands.
- Testing and improving the design of the restraining units to achieve lighter devices.
- Implementing the material model for numerical explicit analysis to be able to simulate the interaction between the elements of the BRBs.
- Use the material model to simulate other all-steel BRBs and study the goodness of fit of the experimental adjustments.
- Carry out specific material test characterization to improve the prediction of the failure point of the material model.
- Simulate entire BRBs, including the restraining unit and the connections, to validate the use of numerical models as virtual tests.

Appendixes

Appendix A

Published paper: A new modular buckling restrained brace for seismic resistant buildings

Daniel Piedrafita; Xavier Cahis; Enric Simon; Jordi Comas. "A new modular buckling restrained brace for seismic resistant buildings". *Engineering Structures*. Vol. 56 (2013) : 1967-1975

<http://dx.doi.org/10.1016/j.engstruct.2013.08.013>

<http://www.sciencedirect.com/science/article/pii/S0141029613003805>

Received 28 January 2013

Revised 6 August 2013

Accepted 10 August 2013

Available online 21 September 2013

Abstract

This paper proposes an innovative BRB as a new energy dissipation device for earthquake resistant buildings. Its steel yielding core is modular, and this very design enables the yielding force and plastic deformation to be adjusted according to building requirements. Based on connecting several Seriated Modules, which are comprised of any constant number of Shear Basic Dissipation Units, deformation is proportional to the number of Seriated Modules and force to the number of Shear Basic Dissipation Units (on the Seriated Modules). Assembling the brace consists of sliding the greased yielding core into the restraining unit and coupling it with pins, thus providing easy inspection or replacement of the dissipation unit if required. Fully-scaled prototypes have been tested under reversal cyclic displacements and the hysteretic response has been proved stable and with a high cumulative ductility. The main parameters are the yielding force and the yielding displacement; which can be predicted with simple expressions. A methodology to design a restraining unit able to tackle of buckling by taking into account the initial sway deformation and the functional gap between the yielding core and the restraining unit is proposed. The hysteretic behavior has been simulated with conventional FEM software.

Keywords

Energy dissipator; Buckling restrained brace; Passive control; Hysteretic damper; Seismic design; Low-cycle fatigue

Appendix B

User material implementation for all-steel BRBs

B.1 Preface

The aim of this appendix is to provide a user's guide and the input file for the User Material implemented in ABAQUS [7] for simulating all-steel BRBs as detailed in Chapter 4. This subroutine has been written by Daniel Piedrafita and Dr. Pere Maimí (University of Girona). First, the main parameters of the input file and the subroutine output meanings are presented and appendix is concluded with the code.

B.1.1 ABAQUS input file

Material properties required for the model are defined in Table B.1 and they consist of three elastic parameters.

E	Young Modulus
ν	Possion coefficient
σ_y	Yielding stress

Table B.1: Material parameters

The properties of the material and the internal variables have to be introduced into the jobfile.inp as is shown Table B.2.

```

*Material, name = BRBsteel
*Depvar
20,
*UserMaterial, constants = 3
E,  $\nu$ ,  $\sigma_y$ 
*Depvar
20
1, EE11, "11 Component of elastic strain"
2, EE22, "22 Component of elastic strain"
3, EE33, "33 Component of elastic strain"
4, EE12, "12 Component of elastic strain"
5, EE13, "13 Component of elastic strain"
6, EE23, "23 Component of elastic strain"
7, EP11, "11 Component of plastic strain"
8, EP22, "22 Component of plastic strain"
9, EP33, "33 Component of plastic strain"
10, EP12, "12 Component of plastic strain"
11, EP13, "13 Component of plastic strain"
12, EP23, "23 Component of plastic strain"
13, APLHA11, "11 Component of kinematic hardening"
14, ALPHA22, "22 Component of kinematic hardening"
15, ALPHA33, "33 Component of kinematic hardening"
16, ALPHA12, "12 Component of kinematic hardening"
17, ALPHA13, "13 Component of kinematic hardening"
18, ALPHA23, "23 Component of kinematic hardening"
19, r, "Amount of plastic flow"
20, D, "Damage scalar"

```

Table B.2: ABAQUS input material parameters and internal variables

B.1.2 State variables

The subroutine has 20 state variables. They are stored as depicted Table B.3.

EE11	STATEV(1)	ε_{11}^E
EE22	STATEV(2)	ε_{22}^E
EE33	STATEV(3)	ε_{33}^E
EE12	STATEV(4)	ε_{12}^E
EE13	STATEV(5)	ε_{13}^E
EE23	STATEV(6)	ε_{23}^E
EP11	STATEV(7)	ε_{11}^P
EP22	STATEV(8)	ε_{22}^P
EP33	STATEV(9)	ε_{33}^P
EP12	STATEV(10)	ε_{12}^P
EP13	STATEV(11)	ε_{13}^P
EP23	STATEV(12)	ε_{23}^P
APLHA11	STATEV(13)	α_{11}
APLHA22	STATEV(14)	α_{22}
APLHA33	STATEV(15)	α_{33}
APLHA12	STATEV(16)	α_{12}
APLHA13	STATEV(17)	α_{13}
APLHA23	STATEV(18)	α_{23}
r	STATEV(19)	r
D	STATEV(20)	D

Table B.3: Internal variable meanings

B.2 Code

```

C *****
C **USER MATERIAL FOR SIMULATING ALL-STEEL BRBS**
C ***** 2012/06/26*****
C *****

C -----
SUBROUTINE UMAT(STRESS, STATEV, DDSDE, SSE, SPD, SCD,
1 RPL, DDSDDT, DRPLDE, DRPLDT,
2 STRAN, DSTRAN, TIME, DTIME, TEMP, DTEMP, PREDEF, DPRED, CMNAME,
3 NDI, NSHR, NTENS, NSTATV, PROPS, NPROPS, COORDS, DROT, PNEWDT,
4 CELENT, DFGRD0, DFGRD1, NOEL, NPT, LAYER, KSPT, KSTEP, KINC)

```

```

INCLUDE 'ABA_PARAM.INC'

CHARACTER*80 CMNAME

DIMENSION STRESS(NTENS),STATEV(NSTATV),
1 DDSDE(NTENS,NTENS),DDSDDT(NTENS),DRPLDE(NTENS),
2 STRAN(NTENS),DSTRAN(NTENS),TIME(2),PREDEF(1),DPRED(1),
3 PROPS(NPROPS),DROT(3,3)

C -----

C -----
C EELAS - ELASTIC STRAINS
C EPLAS - PLASTIC STRAINS
C FLOW - DIRECTION OF PLASTIC FLOW
C -----

DIMENSION EELAS(NTENS),EPLAS(NTENS),FLOW(NTENS),
1 ALPHA(NTENS)

PARAMETER(ZERO=0.DO, ONE=1.DO, TWO=2.DO, THREE=3.DO,
1 SIX=6.DO,ENUMAX=.4999D0, NEWTON=100, TOLER=1.0D-6)

C -----

C PROPS(1) - E
C PROPS(2) - NU
C PROPS(3) - SYIELD
C -----

C ELASTIC PROPERTIES
C -----

EMOD=PROPS(1)
ENU=PROPS(2)
EBULK3=EMOD/(ONE-TWO*ENU)
EG2=EMOD/(ONE+ENU)
EG=EG2/TWO
EG3=THREE*EG
ELAM=(EBULK3-EG2)/THREE
SYIELO=PROPS(3)
NU=0.3

C -----

```

C ELASTIC STIFFNESS

C -----

```

DO K1=1, NDI
DO K2=1, NDI
DDSDDE(K2, K1)=ELAM
END DO
DDSDDE(K1, K1)=EG2+ELAM
END DO
DO K1=NDI+1, NTENS
DDSDDE(K1, K1)=EG
END DO

```

C -----

C RECOVER ELASTIC AND PLASTIC STRAINS AND ROTATE FORWARD

C ALSO RECOVER EQUIVALENT PLASTIC STRAIN

C -----

```

CALL ROTSIG(STATEV(1), DROT, EELAS, 2, NDI, NSHR)
CALL ROTSIG(STATEV(NTENS+1), DROT, EPLAS, 2, NDI, NSHR)
CALL ROTSIG(STATEV(2*NTENS+1), DROT, ALPHA, 1, NDI,
1 NSHR)
EQPLAS=STATEV(3*NTENS+1)

```

C -----

C ELASTIC STRESS

C -----

```

DO K1=1, NTENS
STRESS(K1) = 0.0d0
END DO
DO K1=1, NTENS
EELAS(K1)=EELAS(K1)+DSTRAN(K1)
DO K2=1, NTENS
STRESS(K2)=STRESS(K2)+DDSDDE(K2, K1)*EELAS(K1)
END DO
END DO

```

C -----

C CALCULATE EQUIVALENT VON MISES STRESS

C -----

```

SMISES=(STRESS(1)-ALPHA(1)-STRESS(2)+ALPHA(2))**2
1 +(STRESS(2)-ALPHA(2)-STRESS(3)+ALPHA(3))**2
2 +(STRESS(3)-ALPHA(3)-STRESS(1)+ALPHA(1))**2
DO K1=NDI+1, NTENS

```

```

        SMISES=SMISES+SIX*(STRESS(K1)-ALPHA(K1))**2
    END DO
    SMISES=SQRT(SMISES/TWO)
C -----

C -----
C DETERMINE HARDEING PARAMETERS AND IF ACTIVELY YIELDING
C -----
C HARDENING PARAMETERS
    EMEF=0.07
    EME0=0.3
    EMEP=0.6
    PSIF=192.3
    PSIE=24.59
    PSIL=454.3

C CALCULATE RELATION BETWEEN ISOTROPIC AND
C KINEMATIC HARDENING
    EME=EMEF+(EME0-EMEF)*exp(-EMEP*EQPLAS)
C CALCULATE HARDENING LAW
    SIGMA=SYIELO+PSIF*(1-exp(-PSIE*EQPLAS))+PSIL*EQPLAS
C CALCULATE THE EVOLUTION OF THE ISOTROPIC HARDENING
    CA=EME*(SIGMA-SYIELO)
C CALCULATE THE EVOLUITON OF THE KINEMATIC HARDENING
    BETA=sqrt(TWO/THREE)*((-SIGMA+SYIELO)*(EME0-EMEF)*
1 (-EMEP)*exp(-EMEP*EQPLAS)+(1-EME)*(PSIF*PSIE*
1 exp(-PSIE*EQPLAS)+PSIL))
C DETERMINE IF ACTIVELY YIELDING
    RHS=SMISES-SYIELO-CA
    IF (RHS.GT.0) THEN
C -----

C *****
C ACTIVELY YIELDING
C -----
C SEPARATE THE HYDROSTATIC FROM THE DEVIATORIC STRESS
    SHYDRO=(STRESS(1)+STRESS(2)+STRESS(3))/THREE
C CALCULATE THE FLOW DIRECTION
    DO K1=1,NDI
        FLOW(K1)=(STRESS(K1)-SHYDRO-ALPHA(K1))/SMISES
    END DO
    DO K1=NDI+1, NTENS

```

```

        FLOW(K1)=(STRESS(K1)-ALPHA(K1))/SMISES
        END DO
C -----
C -----
C UPDATE YIELDING SURFACE
C -----
C CALCULATE PLASTIC STRAIN INCREMENT USING NEWTON ITERATION
        DEQPL=0
        DO KEWTON=1, NEWTON
            DEQPL=RHS/(THREE/TWO*(EG2+BETA))
            EQPLAS=EQPLAS+DEQPL
C UPDATE ELASTIC AND PLASTIC DEFORMATIONS
            DO K1=1, NDI
                EPLAS(K1)=EPLAS(K1)+THREE/TWO*FLOW(K1)*DEQPL
                EELAS(K1)=EELAS(K1)-THREE/TWO*FLOW(K1)*DEQPL
            END DO
            DO K1=NDI+1, NTENS
                EPLAS(K1)=EPLAS(K1)+THREE*FLOW(K1)*DEQPL
                EELAS(K1)=EELAS(K1)-THREE*FLOW(K1)*DEQPL
            END DO
C UPDATE HARDENING FUNCTIONS
            EME=emef+(eme0-emef)*exp(-emep*EQPLAS)
            SIGMA=SYIEL0+psif*(1-exp(-psie*EQPLAS))+psil*EQPLAS
            BETA=sqrt(TWO/THREE)*((-SIGMA+SYIEL0)*(eme0-emef)*
1 (-emep)*exp(-emep*EQPLAS)+(1-EME)*(psif*psie*
1 exp(-psie*EQPLAS)+psil))
            DO K1=1, NDI
                ALPHA(K1)=ALPHA(K1)+BETA*sqrt(THREE/TWO)*FLOW(K1)*DEQPL
            END DO
            DO K1=NDI+1, NTENS
                ALPHA(K1)=ALPHA(K1)+BETA*sqrt(THREE/TWO)*FLOW(K1)*DEQPL
            END DO
            CA=EME*(SIGMA-SYIEL0)
C UPDATE STRESS TENSOR
            DO K1=1, NTENS
                STRESS(K1) = 0.0D0
            END DO
            DO K1=1, NTENS
                DO K2=1, NTENS
                    STRESS(K2)=STRESS(K2)+DDSDDE(K2,K1)*EELAS(K1)
                END DO
            END DO

```

```

        END DO
C UPDATE MISES STRESS
        SMISES=(STRESS(1)-ALPHA(1)-STRESS(2)+ALPHA(2))**2
1      +(STRESS(2)-ALPHA(2)-STRESS(3)+ALPHA(3))**2
2      +(STRESS(3)-ALPHA(3)-STRESS(1)+ALPHA(1))**2
        DO K1=NDI+1,NTENS
        SMISES=SMISES+SIX*(STRESS(K1)-ALPHA(K1))**2
        END DO
        SMISES=SQRT(SMISES/TWO)
C UPDATE YIELDING SURFACE
        RHS=SMISES-SYIELO-CA

        IF(ABS(RHS).LT.TOLER) GOTO 10
        END DO

10 CONTINUE
C -----

C -----
C FORMULATE THE JACOBIAN (MATERIAL TANGENT)
C -----
C ELASTIC STRESS
        DO K1=1, NTENS
        STRESS(K1) = 0.0d0
        END DO
        DO K1=1, NTENS
        DO K2=1, NTENS
        STRESS(K2)=STRESS(K2)+DDSDDE(K2,K1)*EELAS(K1)
        END DO
        END DO

C ACTUALIZED ELASTIC STIFFNESS
        DO K1=1,NTENS
        DO K2=1,NTENS
        DDSDDE(K2,K1)=DDSDDE(K2,K1)-9.0*EG**2/(3*EG+3/2*BETA+
1      3/2*((SIGMA-SYIELO)*(eme0-emef)*(-emep)*exp(-emep
2      *EQPLAS)+EME*(psif*psie*exp(-psie*EQPLAS)+psil)))
3      *FLOW(K2)*FLOW(K1)
        END DO
        END DO
C -----

        END IF

```



```

C *****
C *****
C DAMAGE
C -----
C DAMAGE PARAMETERS
  ALPHA2=0.22
  DCR=1
  DO=0.0D0
  RATEPS=70.42D0
  D=STATEV(3*NTENS+2)
  DD=0.0D0
  ALPHA2INV=1/ALPHA2
  ALPHA2EXPO=(ALPHA2-1)*ALPHA2INV
C DAMAGE ACTIVATION
  IF (EQPLAS.GT.0) THEN
    FDD=TWO/THREE*(1+NU)+3*(1-2*NU)*(ABS(SHYDRO/SMISES))**2
    AD=DCR-D
    IF (AD.LT.0) THEN
      AD=0
    END IF
C CALCULATE DAMAGE INCREMENT
    EQPLASOLD=STATEV(3*NTENS+1)
    DD=ALPHA2/LOG(RATEPS)*((DCR-DO)**ALPHA2INV)*
1  AD**ALPHA2EXPO*FDD*0.5D0*(EQPLAS-EQPLASOLD)/
2  (EQPLAS+EQPLASOLD)
    ELSE
      DD=0.0D0
    END IF
C UPDATE DAMAGE VALUE
    D=D+DD
C *****
C -----
C STORE INTERNAL VARIABLES
C -----
C STORE ELASTIC STRAINS, PLASTIC STRAINS AND HARDENING
  DO K1=1, NTENS
    STATEV(K1) = EELAS(K1)
    STATEV(K1+NTENS)=EPLAS(K1)
    STATEV(K1+NTENS*2)=ALPHA(K1)
  END DO

```

C STORE PLASTIC FLOW AND DAMAGE

STATEV(3*NTENS+1)=EQPLAS

STATEV(3*NTENS+2)=D

C -----

RETURN

END

Bibliography

- [1] EN 10025 - 2 : 2004 Technical delivery conditions for non-alloy structural steels, 2004.
- [2] AISC341-05 Seismic Provisions for Structural Steel, 2005.
- [3] UNE-EN 1993-1-1:2005: Eurocode 3.1.1 General structural rules, 2005.
- [4] Código Técnico de la Edificación (CTE) Documento Básico Seguridad Estructural Acero (DB-SE A), 2006.
- [5] EN15129 Anti-seismic devices, 2009.
- [6] *ABAQUS version 6.9: ABAQUS User's Manual, SIMULIA World Headquarters, 166 Valley Street, Providence, RI 02909, USA., 2009.*
- [7] *ABAQUS version 6.12: ABAQUS User's Manual, SIMULIA World Headquarters, Rissing Sun Mills 166 Valley Street, Providence, RI 02909-2499, USA., 2012.*
- [8] *MATLAB version R2013a, The MathWorks Inc., Natick, Massachusetts, 2013.*
- [9] Ian D Aiken, Douglas K Nims, Andrew S Whittaker, and James M Kelly. Testing of Passive Energy Dissipation Systems. *Earthquake Spectra*, 9(3), 1993.
- [10] Amadeo Benavent-Climent. A brace-type seismic damper based on yielding the walls of hollow structural sections. *Engineering Structures*, 32(4):1113–1122, APR 2010. ISSN 0141-0296. doi: {10.1016/j.engstruct.2009.12.037}.

-
- [11] C. Black, N. Martin, and I. Aiken. Component testing, stability analysis and characterization of buckling restrained unbounded braces. Technical report, Pacific earthquake engineering research center, College of Engineering, University of California, Berkeley, 2002.
- [12] C Black, N Makris, and I Aiken. Component testing, seismic evaluation and characterization of buckling-restrained braces. *Journal of Structural Engineering*, 130:880–894, 2004.
- [13] Friederich Bleich. *Buckling strength of metal structures*. McGraw-Hill, 1952.
- [14] N. Bonora and G.M. Newaz. Low cycle fatigue life estimation for ductile metals using a nonlinear continuum damage mechanics model. *International Journal of Solids and Structures*, 35(16):1881–1894, June 1998. ISSN 00207683. doi: 10.1016/S0020-7683(97)00139-X.
- [15] Nicola Bonora. A nonlinear CDM model for ductile failure. *Engineering Fracture Mechanics*, 58(I):11–28, 1997.
- [16] Nicola Bonora, Domenico Gentile, a. Pirondi, and Golam Newaz. Ductile damage evolution under triaxial state of stress: theory and experiments. *International Journal of Plasticity*, 21(5):981–1007, May 2005. ISSN 07496419. doi: 10.1016/j.ijplas.2004.06.003.
- [17] Ian G. Buckle. Passive control of structures for seismic loads. *12th World Conference on Earthquake Engineering*, 2000.
- [18] Xavier Cahís. *Development of a new energy dissipator for seismic design. Numerical analysis and experimental validation of its behavior*. PhD thesis, Universitat Politècnica de Catalunya, 2001.
- [19] Xavier Cahís, Lluís Torres, and L.M Bozzo. An innovative elasto-plastic energy dissipator for the structural and non-structural buildings protection. *12th World Conference on Earthquake Engineering*, 2000.
- [20] Cheng-Cheng Chen. Recent advances of seismic design of steel buildings in taiwan. *International Training Programs for Seismic Design of Buildings Structures*, 2002.

-
- [21] Chung-Che Chou and Sheng-Yang Chen. Subassemblage tests and finite element analyses of sandwiched buckling-restrained braces. *Engineering Structures*, 32(8):2108–2121, August 2010. ISSN 01410296. doi: 10.1016/j.engstruct.2010.03.014.
- [22] T K Datta and Hauz Khas. A STATE-OF-THE-ART REVIEW ON ACTIVE CONTROL OF STRUCTURES. 40(430):1–17, 2003.
- [23] Satyendra Kumar Ghosh and David Anthony Fanella. *Seismic and Wind Design of Concrete Buildings:(2000 IBC, ASCE 7-98, ACI 318-99)*. Kaplan AEC Engineering, 2003.
- [24] M. Iwata. Applications-design of buckling restrained braces in japan. *13th World Conference on Earthquake Engineering*, Paper 3208, 2004.
- [25] Mamoru Iwata and Masatoshi Murai. Buckling-restrained brace using steel mortar planks; performance evaluation as a hysteretic damper. *Earthquake Engineering & Structural Dynamics*, 35(14):1807–1826, NOV 25 2006. ISSN 0098-8847. doi: {10.1002/eqe.608}.
- [26] Y.K Ju, M.H. Kim, J. Kim, and S.D Kim. Component tests of buckling-restrained braces with unconstrained length. *Engineering Structures*, 31: 501–516, 2009.
- [27] E.P. Kasai, K. Popov. Cyclic web buckling control for shear link beams. *Journal of Structural Engineering*, 110 (3):505–523, 1986.
- [28] Dongkeon Kim, Gary F. Dargush, and Cemal Basaran. A cyclic two-surface thermoplastic damage model with application to metallic plate dampers. *Engineering Structures*, 52:608–620, July 2013. ISSN 01410296. doi: 10.1016/j.engstruct.2013.02.030.
- [29] T Kobori, Y Miura, E Fukuzwa, T Yamada, T Arita, Y Takenaka, N Miyagawa, N Tanaka, and T Fukumoto. Development and application of hysteresis steel dampers. *Earthquake Engineering, Tenth World Conference, Balkema, Rotterdam*, 1992.
- [30] Perrin G. Devaux J Leblond, J.-B. An improved Gurson-type model for hardenable ductile metals. *European Journal of Mechanics*, 14 (4):499–527, 1995.

-
- [31] Jean Lemaitre and Rodrigue Desmorat. *Engineering Damage Mechanics*. Springer, 2010.
- [32] Walterio A. López and Rafael Sabelli. Seismic Design of Buckling-Restrained Braced Frames. Technical Report July, Structural Steel Educational Council, 2004.
- [33] F. López-Almansa, J.C. Castro-Medina, and S. Oller. A numerical model of the structural behavior of buckling-restrained braces. *Engineering Structures*, 41:108–117, August 2012. ISSN 01410296. doi: 10.1016/j.engstruct.2012.03.045.
- [34] Jacob Lubliner. *Plasticity Theory*. University of California, 1990.
- [35] X Martinez, Oller.S, L.G Barbu, and H.A Barbat. Analysis of ultra low cycle fatigue problems with the barcelona plastic damage model. In *XII International Conference on Computational Plasticity. Fundamentals and Applications. COMPLAS XII*, 2013.
- [36] James Newell, Chia-Ming Uang, and Gianmario Benzoni. Subassemblage testing of corebrace buckling-restrained braces (g series). final report to corebrace,llc. Technical report, Department of Structural Engineering. University of California, 2006.
- [37] Sang-Hoon Oh, Young-Ju Kim, and Hong-Sik Ryu. Seismic performance of steel structures with slit dampers. *Engineering Structures*, 31(9):1997 – 2008, 2009. ISSN 0141-0296. doi: 10.1016/j.engstruct.2009.03.003.
- [38] Niels Saabye Ottosen and Matti Ristinmaa. *The Mechanics of Constitutive Modeling*. Elsevier Ltd., 2005.
- [39] G. Palazzo, F. Lopez-Almansa, X. Cahis, and F. Crisafulli. A low-tech dissipative buckling restrained brace. Design, analysis, production and testing. *Engineering Structures*, 31(9):2152–2161, SEP 2009. ISSN 0141-0296. doi: {10.1016/j.engstruct.2009.03.015}.
- [40] J Park, J Lee, and J Kim. Cyclic test of buckling restrained braces composed of square steel rods and steel tube. *Steel and Composite Structures*, 13: 423.436, 2012.

-
- [41] D. Piedrafita, X. Cahis, E. Simon, and J. Comas. A new modular buckling restrained brace for seismic resistant buildings. *Engineering Structures*, 56:1967–1975, November 2013. ISSN 01410296. doi: 10.1016/j.engstruct.2013.08.013.
- [42] A. Pironi, N. Bonora, D. Steglich, W. Brocks, and D. Hellmann. Simulation of failure under cyclic plastic loading by damage models. *International Journal of Plasticity*, 22(11):2146–2170, November 2006. ISSN 07496419. doi: 10.1016/j.ijplas.2006.03.007.
- [43] G. Song, N. Ma, and H.-N. Li. Applications of shape memory alloys in civil structures. *Engineering Structures*, 28(9):1266–1274, July 2006. ISSN 01410296. doi: 10.1016/j.engstruct.2005.12.010.
- [44] G. F. Soong, T.T Dargush. *Structural Engineering Handbook*. CRC Press, 1999.
- [45] T T Soong and Jr B F Spencer. Supplemental energy dissipation : state-of-the-art and state-of-the- practice. *Engineering Structures*, 24:243–259, 2002.
- [46] Jr B F Spencer and S Nagarajaiah. State of the Art of Structural Control. *Journal of Structural Engineering*, 129(July):845–856, 2003.
- [47] M. D. Symans, F. a. Charney, a. S. Whittaker, M. C. Constantinou, C. a. Kircher, M. W. Johnson, and R. J. McNamara. Energy Dissipation Systems for Seismic Applications: Current Practice and Recent Developments. *Journal of Structural Engineering*, 134(1):3–21, January 2008. ISSN 0733-9445. doi: 10.1061/(ASCE)0733-9445(2008)134:1(3).
- [48] K. Tsai, Y. Lai, V. Hwang, and C. Lin. Research and application of double-core buckling restrained braces in Taiwan. *13th World Conference on Earthquake Engineering*, Paper 2179, 2004.
- [49] C-M Uang, M. Nakashima, and Tsai K. Research and application of buckling restrained braced frames. *Steel Structures*, 4:301–313, 2004.
- [50] Atushi Watanabe, Yasuyoshi Hitomi, Eiichiro Saeki, Akira Wada, and Morihisa Fujimoto. Properties of brace encased in buckling-restraining concrete and steel tube. *Proceedings of Ninth World Conference on Earthquake Engineering*, IV:719–724, 1988.

-
- [51] Chuan Xia and Robert D. Hanson. Influence of ADAS Element Parameters on Building Seismic Response. *Journal of Structural Engineering*, 118(7):1903–1918, 1992.
- [52] Qiang Xie. State of the art of buckling-restrained braces in Asia. *Journal of Constructional Steel Research*, 61(6):727–748, June 2005. ISSN 0143974X. doi: 10.1016/j.jcsr.2004.11.005.
- [53] Fusahito Yoshida. A constitutive model of cyclic plasticity. *International Journal of Plasticity*, 16(3-4):359–380, January 2000. ISSN 07496419. doi: 10.1016/S0749-6419(99)00058-3.
- [54] Fusahito Yoshida and Takeshi Uemori. A model of large-strain cyclic plasticity describing the Bauschinger effect and workhardening stagnation. *International Journal of Plasticity*, 18(5-6):661–686, October 2002. ISSN 07496419. doi: 10.1016/S0749-6419(01)00050-X.
- [55] Fusahito Yoshida, Takeshi Uemori, and Kenji Fujiwara. Elasticplastic behavior of steel sheets under in-plane cyclic tensioncompression at large strain. *International Journal of Plasticity*, 18(5-6):633–659, October 2002. ISSN 07496419. doi: 10.1016/S0749-6419(01)00049-3.
- [56] Junxian Zhao, Bin Wu, and Jinping Ou. A novel type of angle steel buckling-restrained brace: Cyclic behavior and failure mechanism. *Earthquake Engineering & Structural Dynamics*, 40(10):1083–1102, AUG 2011. ISSN 0098-8847. doi: {10.1002/eqe.1071}.
- [57] Alessandro Zona and Andrea Dall’Asta. Elastoplastic model for steel buckling-restrained braces. *Journal of Constructional Steel Research*, 68(1):118–125, January 2012. ISSN 0143974X. doi: 10.1016/j.jcsr.2011.07.017.



AMADE

ANALYSIS AND ADVANCED MATERIALS
FOR STRUCTURAL DESIGN